

**STATE ESTIMATION OF AN UNMANNED
GROUND VEHICLE USING INEXPENSIVE
SENSORS**

by

Noah Johnson

A Thesis

Submitted to the Division of Natural Sciences
New College of Florida
in partial fulfillment of the requirements for the degree
Bachelor of Arts
under the sponsorship of Professor Gary Kalmanovich

Sarasota, Florida
August 2017

Acknowledgments

I'd like to thank my thesis sponsor Dr. Gary Kalmanovich, for his advice and giving me the freedom to explore this passion project. I'd also like to thank Dr. David Gillman for his advice and editing help. And special thanks to Nikolas "Waka Flocka" Wojtalewicz for his mathematical expertise.

Lastly, thanks to New College of Florida for providing the funding and environment to make this thesis possible.

Contents

Acknowledgments	ii
Contents	iii
Abstract	vi
Introduction	3
1 Theory	4
1.1 Probability Theory Background	4
1.2 Bayes Filter	7
1.2.1 Scenario	7
1.2.2 Derivation	8
1.3 Extended Kalman Filter	10
1.3.1 Matrix Calculus	13
1.3.2 Derivation	19
1.3.3 Remarks	34
2 Hardware	35
2.1 Specific Hardware Used	35

2.2	Construction	39
2.3	Power	41
3	Arduino	45
3.1	Background	45
3.1.1	Servo Control Pulses	46
3.2	Arduino Uno Connections	46
3.2.1	Hardware Interrupt Pins	46
3.2.2	Digital Pin Connections	47
3.3	Motor Driver's Configuration	48
3.4	Arduino Sketch	49
3.4.1	Ultrasonic Sensor	50
3.4.2	Servo	50
3.4.3	Quadrature Encoders	52
4	ROS	60
4.1	ROS Basics	60
4.1.1	Messaging	60
4.1.2	Packages	61
4.1.3	Frames and Transforms	62
4.2	rosserial	65
4.2.1	rosserial_arduino	66
4.2.2	rosserial_python	68
4.3	differential_drive	69

4.3.1	diff_odom	69
4.3.2	twist_to_motors	73
4.3.3	pid_velocity	74
4.3.4	virtual_joystick	75
4.4	Ros Sensors App	76
4.4.1	GPS	76
4.4.2	IMU	77
4.5	robot_localization	78
5	Field Test	80
5.1	Experiment Design	80
5.2	Results	81
Conclusion		87

State Estimation of an Unmanned Ground Vehicle Using Inexpensive Sensors

Noah Johnson

New College of Florida, 2017

Submitted to the Division of Natural Sciences
on August 10, 2017, in partial fulfillment of the
requirements for the degrees of
Bachelor of Arts in Computer Science
and
Bachelor of Arts in Applied Mathematics

Abstract

Autonomous navigation is an important emerging technology with applications in warehouse automation, shipping, and personal navigation. An important step in being able to enter this new field is working with physical hardware. However, hands-on experimentation may prove too expensive for individuals at the undergraduate level, with common research platforms costing several thousand dollars. In this thesis, I present a design for a cheap ground vehicle capable of fusing sensor data into a local state estimate, the first step of navigation. Costs were minimized by using personal components most college students already own, namely a personal laptop and smartphone. This should be an effective base to allow wider entry into autonomous navigation research.

Professor Gary Kalmanovich

August 10, 2017

Introduction

Navigation of a robot involves localizing where the robot is with respect to its environment, finding a path from where it currently is to where it would like to be, executing commands to follow that path, and dynamically reacting to obstacles to avoid collisions. While the robot design presented in this thesis is capable of performing all of these tasks, only the first - localization - has been implemented.

In order for a robot to localize itself with respect to its environment, it must either already know its environment via a static map, or dynamically generate a map of its surroundings. This latter approach is known as the simultaneous localization and mapping (SLAM) problem, and the most common algorithms used to solve it involve the use of ranging sensors. Ranging sensors measure the distance between the robot and surrounding obstacles.

In this project a static map was assumed to exist, where the map used is the Universal Transverse Mercator (UTM) 2D projection of a coordinate system onto the Earth's surface. A Global Positioning System (GPS) receiver was used for noisy global position information, and localization was implemented with respect to this map. Therefore ranging sensors - though purchased - were not used.

The rover's design is carefully laid out by this thesis in the hope that other students or individuals interested in experimenting with autonomous navigation will be able to replicate the construction. The cheap material cost may help ease the financial burden for those who wish for hands-on experience in this field. The design consists of a four-wheeled skid-steering aluminum rover base, an Arduino microcontroller, and motor driver. It is controlled by a laptop connected via USB. Sensors available include two motor rotary encoders, a mobile smartphone, and an ultrasonic distance sensor. The Arduino acts as a low-level robotic controller, sending wheel encoder and range data to the laptop, and accepting motor velocity commands. An Android app publishes Intertial Measurement Unit (IMU) and GPS data from the mobile phone, and the laptop fuses these readings into a state estimation of pose and velocity using an extended Kalman filter.

The sensors available are limited in precision, but were chosen for their cheap cost and wide availability.

Rather than purchasing separate IMU and GPS chips to interface with the Arduino microcontroller, we used the built-in sensors on a smartphone. These built-in sensors are less accurate than their external counterparts, but in many cases present no additional cost to acquire for a college student.

Infrared (IR) sensors are cheap ranging sensors common in small robotics projects. However, this rover was designed to work outdoors during the day, and the ambient IR radiation from the sun makes these sensors unusable. Meanwhile light detection and ranging (LIDAR) sensors are highly expensive ranging sensors which are considered the industry standard for high resolution, high accuracy point cloud mapping in a

360 degree arc. Due to the financial constraints of this thesis, these range sensors are out of the question. So a third option, the ultrasonic sensor, was chosen. Ultrasonic sensors are medium-distance ranging sensors which emit high-frequency sonic pulses and measure the echo time. They are capable of detecting objects in a cone shape in front of them. They have reduced accuracy in rain or snow, and can suffer from confusing double echoes. However, they are nearly as inexpensive as IR sensors, and by panning back and forth, can slowly give a 180 degree distance measurement.

The rest of this thesis is structured as follows.

Chapter 1 covers the probability theory behind the extended Kalman filter, which is an iterative algorithm used to fuse noisy sensor data into a local state estimate for the rover. It may be skipped if one is not interested in the mathematical details. Chapter 2 describes the hardware components used in this project, their electrical connections, and the general design. Chapter 3 continues the description of physical connections with respect to the Arduino circuit board, and also describes the software which runs on that board and how it interfaces with the rest of the system. Chapter 4 gives a brief overview of the Robot Operating System (ROS), and how it is used in this project. It then touches on the distinct software processes that make up the system. Chapter 5 describes the results of an experimental localization test run conducted with the rover.

Chapter 1

Theory

This section will dive into the mathematical theory behind the recursive state estimator used in this project, the Extended Kalman Filter. Steps have been taken to carefully explain every computation made for the less mathematically inclined. This section is largely based on chapters 1-3 of the book Probabilistic Robotics, which the interested reader should view for a broader look at the same material. [probabilisticRobotics].

1.1 Probability Theory Background

Robots work with stochastic data, and so probability theory is vital to understanding their inner workings. Here we will review some elementary probability theory results which will be needed in this chapter.

Random variables are objects from which specific numbers may be observed. Let X be a continuous random variable - that is, observations of X are real numbers. We

will represent the probability of observing any particular real number x from X as $p(X = x) \equiv p(x)$. This defines a function $p : \mathbb{R} \rightarrow \mathbb{R}$ representing the distribution of probabilities for the real numbers. Throughout this chapter, we will refer to such functions as PDFs (probability density functions). Note the basic result that for every PDF p constructed from a random variable X , $\int p(x)dx = 1$, which is to say that the observed value from X will be a real number with 100% certainty.

An important tool for describing PDFs is the expectation. We will define $E[X]$ to be the expected value, or arithmetic mean of, X . Note that the expectation operator is linear: $E[\alpha X + \beta Y] = \alpha E[X] + \beta E[Y]$.

For two random variables X and Y , we will define their covariance to be

$$cov(X, Y) = E[(X - E[X])(Y - E[Y])]$$

. This gives a measure of the linear relationship between X and Y .

The same concepts may be scaled up to random vectors, which are n -dimensional collections of random variables. Then $X = (X_1, X_2, \dots, X_n)^T$, and $p : \mathbb{R}^n \rightarrow \mathbb{R}$ still defines a PDF. The expectation becomes

$$E[X] = \begin{pmatrix} E[X_1] \\ \vdots \\ E[X_n] \end{pmatrix}$$

and we can define a covariance matrix Σ for the random vector:

$$\Sigma = E[(X - E[X])(X - E[X])^T] = \begin{pmatrix} cov(X_1, X_1) & \dots & cov(X_1, X_n) \\ & \ddots & \\ cov(X_n, X_1) & \dots & cov(X_n, X_n) \end{pmatrix}$$

Now consider three random variables: X, Y, and Z. Define the joint distribution $p(X = x \text{ and } Y = y \text{ and } Z = z) \equiv p(x, y, z)$, and the conditional probability $p(X = x \text{ given that } Y = y \text{ and } Z = z) \equiv p(x | y, z)$. The conditional probability is defined to be

$$p(x | y, z) = \frac{p(x, y, z)}{p(y, z)} \quad (1.1)$$

The *Law of Total Probability* states that $p(x) = \int p(x, y)dy$. Extending this law to use a third random variable Z, and incorporating Equation 1.1, we end up with the following equation:

$$p(x | z) = \int p(x, y | z)dy = \int p(y, z)p(x | y, z)dy \quad (1.2)$$

Using equations 1.2 and 1.1, one can derive a formula known as Bayes' Rule.

$$p(x | y, z) = \frac{p(x, y, z)}{p(y, z)} = \frac{p(y, x, z)}{p(x, z)} * \frac{p(x, z)}{p(y, z)} = \frac{p(y | x, z)p(x, z)}{p(y | z)} \quad (1.3)$$

In the future this will prove to be a useful tool to update a PDF with new information. When presented with new information that $Y = y$, one may use Bayes' Rule to

transform the current PDF $p(x | z)$ into the new posterior PDF $p(x | y, z)$.

1.2 Bayes Filter

1.2.1 Scenario

Now, back to the inner workings of our rover. Consider the general case of a robot which uses some array of sensors to gather information about its environment. The robot wishes to use these measurements to estimate its current state, where the state is a collection of variables of interest (e.g. position, orientation, velocity, acceleration, etc.).

For simplicity, let us consider the rover to operate in discrete time steps ($t = 0, 1, 2, \dots$). We can encode all state variables of interest in the vector $x_t = (x_{1t}, x_{2t}, \dots, x_{nt})^T$. Similarly, let $z_t = (z_{1t}, z_{2t}, \dots, z_{kt})^T$ represent a sensor measurement at time t . For both of these vectors we will use the compact notation $a_{1:t} = a_1, a_2, \dots, a_t$ to denote the set of all vectors up to and including time t .

The robot wishes to know x_t , however this true state is hidden. It only has access to raw sensor data in the form of $z_{1:t}$. Sensor measurements always contain some level of noise due to ambient interference, no matter how precise the hardware. Thus each of these measurements will have some amount of error, and the robot will need to account for this in its state estimate. The robot can do this by constructing a PDF assigning a probability to every possible realization of x_t . This PDF will represent the robot's belief in its current state, and should be conditioned on all available data.

Thus we will define the robot's belief distribution to be:

$$\text{bel}(x_t) = p(x_t | z_{1:t}) \quad (1.4)$$

1.2.2 Derivation

Now we must figure out how to compute $\text{bel}(x_t)$. Let us start by using Bayes' Rule to rewrite $\text{bel}(x_t)$:

$$\text{bel}(x_t) = p(x_t | z_{1:t}) = \frac{p(z_t | x_t, z_{1:t-1})p(x_t | z_{1:t-1})}{p(z_t | z_{1:t-1})}$$

In order to continue, we will need to simplify $p(z_t | x_t, z_{1:t-1})$. Here we will make an important assumption. We will assume that the state x_t satisfies the Markov property: that is, x_t perfectly encapsulates all current and prior information [robot_localization_paper]. Thus if x_t is known, then $z_{1:t}$ are redundant, i.e. $p(z_t | x_t, z_{1:t}) = p(z_t | x_t)$.

This assumption lets us remove consideration of past sensor measurements, and to rewrite the belief distribution as:

$$\text{bel}(x_t) = \frac{p(z_t | x_t)p(x_t | z_{1:t-1})}{p(z_t | z_{1:t-1})}$$

Notice that $p(z_t | z_{1:t-1})$ is a constant with respect to x_t . Thus it makes sense to

define $\eta = (p(z_t | z_{1:t-1}))^{-1}$ and rewrite the belief distribution as:

$$\text{bel}(x_t) = \eta p(z_t | x_t) p(x_t | z_{1:t-1})$$

Notice that $\text{bel}(x_t)$ is a PDF, so it must integrate to 1. η acts as a normalizing constant enforcing this constraint.

Now $\text{bel}(x_t)$ has been split into two distributions of interest. Looking closely one may notice that $p(x_t | z_{1:t-1})$ is simply our original belief distribution, Eq. 1.4, but not conditioned on the most recent sensor measurement z_t . Let us refer to this distribution as $\overline{\text{bel}}(x_t)$, and break it down further using the *Law of Total Probability* (Eq. 1.2) and our Markov assumption:

$$\begin{aligned} \overline{\text{bel}}(x_t) &= p(x_t | z_{1:t-1}) \\ &= \int p(x_t | x_{t-1}, z_{1:t-1}) p(x_{t-1} | z_{1:t-1}) dx_{t-1} && \text{(by Eq. 1.2)} \\ &= \int p(x_t | x_{t-1}) p(x_{t-1} | z_{1:t-1}) dx_{t-1} && \text{(by Markov assumption)} \\ &= \int p(x_t | x_{t-1}) \text{bel}(x_{t-1}) dx_{t-1} && \text{(by Eq. 1.4)} \end{aligned}$$

We have arrived at a recursive definition of $\text{bel}(x_t)$ with respect to $\text{bel}(x_{t-1})$! As long as $p(x_t | x_{t-1})$ and $p(z_t | x_t)$ are known, we can recursively calculate $\text{bel}(x_t)$ from some starting belief $\text{bel}(x_0)$.

$p(x_t | x_{t-1})$ defines a stochastic model for the robot's state, determining how the robot's state will evolve over time. This PDF will be referred to as the *state transition probability* [probabilisticRobotics].

$p(z_t | x_t)$ also defines a stochastic model, modeling the sensor measurements z_t as noisy projections of the robot's state. This PDF will be referred to as the *measurement probability* [probabilisticRobotics].

Once we assume the *state transition probability* and *measurement probability* PDFs are known, we can finally construct the algorithm known as Bayes' Filter:

Algorithm 1 Bayes Filter

```

1: function BAYESFILTERITERATE( bel( $x_{t-1}$ ),  $z_t$  )
2:    $\bar{\text{bel}}(x_t) = \int p(x_t | x_{t-1})\text{bel}(x_{t-1})dx_{t-1}$ 
3:    $\text{bel}(x_t) = \eta p(z_t | x_t)\bar{\text{bel}}(x_t)$ 
4:   Set  $\int \text{bel}(x_t)dx = 1$ , and solve for  $\eta$ 
5:   Use  $\eta$  to normalize  $\text{bel}(x_t)$ 
6:   return  $\text{bel}(x_t)$ 
7: end function
```

1.3 Extended Kalman Filter

The most widely used algorithm implementing Bayes Filter is the Extended Kalman Filter (EKF). This filter approximates the PDFs found in Bayes Filter with multivariate normal distributions. This class of PDFs are unimodal, and have the form

$$p(x) = N(x; E[X], \Sigma) = \det(2\pi\Sigma)^{-\frac{1}{2}} * \exp\left\{-\frac{1}{2}(x - E[X])^T \Sigma^{-1} (x - E[X])\right\} \quad (1.5)$$

where $E[X]$ and Σ are the mean and covariance matrix of the random vector X , as described in section 1.1. Notice that the mean and covariance matrix are sufficient to uniquely define any particular normal distribution, and so the EKF only needs to keep track of a vector and matrix per PDF. So the belief distribution can be

totally described by the best estimate for the state vector and the uncertainty in that estimate:

$$\text{bel}(x_t) = N(x_t; \mu_t, \Sigma_t) \quad (1.6)$$

where $\mu_t = E[X_t]$ is the mean or best estimate, and Σ_t is the covariance matrix or uncertainty. These are the values which our new algorithm will try to compute; doing so will completely describe $\text{bel}(x_t)$.

Recall that Algorithm 1 (Bayes' Filter) requires that the state transition PDF ($p(x_t | x_{t-1})$) be given. So let us assume that the evolution of state is known via some model

$$x_t = g(x_{t-1}) + \epsilon_t$$

where $g : \mathbb{R}^n \rightarrow \mathbb{R}^n$ is some arbitrary function defining how the state evolves, and ϵ_t is additive noise in the model. We will define ϵ_t to be a random vector of normal distribution with mean 0 and covariance matrix R_t .

We will linearize this model by a first-order Taylor series approximation around the current best estimate, μ_{t-1} .

$$\begin{aligned} g(x_{t-1}) &\approx g(\mu_{t-1}) + \frac{\partial g(\mu_{t-1})}{\partial x_{t-1}}(x_{t-1} - \mu_{t-1}) \\ &= g(\mu_{t-1}) + G_t(x_{t-1} - \mu_{t-1}) \end{aligned}$$

where

$$G_t = \begin{bmatrix} \frac{\partial g_1(\mu_{t-1})}{\partial x_{1_{t-1}}} & \cdots & \frac{\partial g_1(\mu_{t-1})}{\partial x_{n_{t-1}}} \\ \vdots & \ddots & \vdots \\ \frac{\partial g_n(\mu_{t-1})}{\partial x_{1_{t-1}}} & \cdots & \frac{\partial g_n(\mu_{t-1})}{\partial x_{n_{t-1}}} \end{bmatrix}$$

is the Jacobian of g evaluated at μ_{t-1} . Then rewriting the model, we have

$$x_t \approx g(\mu_{t-1}) + G_t(x_{t-1} - \mu_{t-1}) + \epsilon_t$$

Then the mean of the state transition PDF is

$$\begin{aligned} E[x_t \mid x_{t-1}] &\approx E[g(\mu_{t-1}) + G_t(x_{t-1} - \mu_{t-1}) + \epsilon_t \mid x_{t-1}] \\ &= E[g(\mu_{t-1}) + G_t(x_{t-1} - \mu_{t-1}) \mid x_{t-1}] + E[\epsilon_t \mid x_{t-1}] \quad (\text{by linearity of } E[X]) \\ &= E[g(\mu_{t-1}) + G_t(x_{t-1} - \mu_{t-1}) \mid x_{t-1}] \quad (\text{by the definition of } \epsilon_t) \\ &= g(\mu_{t-1}) + G_t(x_{t-1} - \mu_{t-1}) \end{aligned}$$

and covariance matrix

$$\begin{aligned}
& E[(x_t - E[x_t])(x_t - E[x_t])^T \mid x_{t-1}] \\
& \approx E[(g(\mu_{t-1}) + G_t(x_{t-1} - \mu_{t-1}) + \epsilon_t - g(\mu_{t-1}) - G_t(x_{t-1} - \mu_{t-1})) \\
& * (g(\mu_{t-1}) + G_t(x_{t-1} - \mu_{t-1}) + \epsilon_t - g(\mu_{t-1}) - G_t(x_{t-1} - \mu_{t-1}))^T \mid x_{t-1}] \\
& = E[\epsilon_t \epsilon_t^T \mid x_{t-1}] = E[(\epsilon_t - 0)(\epsilon_t - 0)^T \mid x_{t-1}] \\
& = E[(\epsilon_t - E[\epsilon_t \mid x_{t-1}])(\epsilon_t - E[\epsilon_t \mid x_{t-1}])^T \mid x_{t-1}] = R_t
\end{aligned}$$

and so its Gaussian distribution is

$$p(x_t \mid x_{t-1}) \approx N(x_t; g(\mu_{t-1}) + G_t(x_{t-1} - \mu_{t-1}), R_t) \quad (1.7)$$

1.3.1 Matrix Calculus

For the mathematical derivation of the EKF which lies ahead, we will be working with matrix calculus.

For the benefit of the unfamiliar reader, here we will restate some elementary results which will be needed to follow along.

For $A, B \in \mathbb{R}^{n \times n}$:

$$(AB)^T = B^T A^T \quad (1.8)$$

$$(A + B)^T = A^T + B^T \quad (1.9)$$

$$A \text{ is symmetric} \implies A^T = A \quad (1.10)$$

$$A \text{ is symmetric} \implies A^{-1} \text{ is symmetric} \quad (1.11)$$

Lemma 1.3.1. *For $x \in \mathbb{R}^n$ and $A \in \mathbb{R}^{n \times n}$, A symmetric,*

$$\frac{\partial(x^T A x)}{\partial x} = 2Ax$$

Proof.

Define $f : \mathbb{R}^n \rightarrow \mathbb{R}$, $f(x) = x^T A x$

$$x = \begin{pmatrix} x_1 \\ \vdots \\ x_n \end{pmatrix}, \frac{\partial f}{\partial x} = \begin{pmatrix} \frac{\partial f}{\partial x_1} \\ \vdots \\ \frac{\partial f}{\partial x_n} \end{pmatrix}, e_i = \begin{pmatrix} 0 \\ \vdots \\ 1 \\ \vdots \\ 0 \end{pmatrix}$$

For $h \in \mathbb{R}$,

$$\begin{aligned} \frac{\partial f}{\partial x_i} &= \lim_{h \rightarrow 0} \frac{f(x + h e_i) - f(x)}{h} = \lim_{h \rightarrow 0} \frac{(x + h e_i)^T A (x + h e_i) - x^T A x}{h} \\ &= \lim_{h \rightarrow 0} \frac{x^T A x + h * x^T A e_i + h * e_i^T A x + h^2 * e_i^T A e_i - x^T A x}{h} \\ &= \lim_{h \rightarrow 0} \frac{h[x^T A e_i + e_i^T A x + h * e_i^T A e_i]}{h} = \lim_{h \rightarrow 0} (x^T A e_i + e_i^T A x + h * e_i^T A e_i) \\ &= x^T A e_i + e_i^T A x = e_i^T A^T x + e_i^T A x \quad (x^T A e_i \text{ is } 1 \times 1 \therefore x^T A e_i \text{ is symmetric}) \\ &= e_i^T (A^T + A) x = e_i^T (A + A) x = e_i^T (2 A x) \quad (\text{by symmetry of } A) \end{aligned}$$

Which tells us that the i^{th} component of $\frac{\partial f}{\partial x}$ is equal to the i^{th} component of $2 A x$.

$$\therefore \frac{\partial f}{\partial x} = 2 A x$$

□

Lemma 1.3.2. For $x, a \in \mathbb{R}^n$, $\frac{\partial(x^T a)}{\partial x} = \frac{\partial(a^T x)}{\partial x} = a$

Proof.

$$\frac{\partial(a^T x)}{\partial x} = \begin{pmatrix} \frac{\partial(a^T x)}{\partial x_1} \\ \vdots \\ \frac{\partial(a^T x)}{\partial x_n} \end{pmatrix} = \begin{pmatrix} \frac{\partial(a_1 x_1 + \dots + a_n x_n)}{\partial x_1} \\ \vdots \\ \frac{\partial(a_1 x_1 + \dots + a_n x_n)}{\partial x_n} \end{pmatrix} = \begin{pmatrix} a_1 \\ \vdots \\ a_n \end{pmatrix} = a$$

$a^T x$ has dimension 1 by 1, $\therefore a^T x = (a^T x)^T = x^T a$

$$\implies \frac{\partial(a^T x)}{\partial x} = \frac{\partial(x^T a)}{\partial x} = a$$

□

Lemma 1.3.3. Let $f : \mathbb{R}^n \rightarrow \mathbb{R}$ be a quadratic function given by

$$f(x) = x^T A x + B x + C$$

where A is a symmetric matrix of dimension $n \times n$, B is a matrix of dimension $1 \times n$,

and $C \in \mathbb{R}$. Then

$$f(x) = f(a) + \frac{1}{2}(x - x^*)^T \frac{\partial^2 f}{\partial x^2}(x - x^*)$$

where $\frac{\partial f}{\partial x}(x^*) = 0$.

Note: This is a higher-dimensional application of Taylor's Theorem.

Proof.

$$\begin{aligned}\frac{\partial f}{\partial x} &= \frac{\partial(x^T Ax)}{\partial x} + \frac{\partial(Bx)}{\partial x} + \frac{\partial(C)}{\partial x} = 2Ax + B^T && \text{(by prior Lemmas)} \\ \therefore \frac{\partial f}{\partial x} &= 0 \implies x^* = -\frac{1}{2}A^{-1}B^T\end{aligned}$$

$$\frac{\partial^2 f}{\partial x^2} = \frac{\partial(2Ax)}{\partial x} + \frac{\partial(B^T)}{\partial x} = 2A^T = 2A \quad \text{(by symmetry of A)}$$

$$\begin{aligned}f(a) + \frac{1}{2}(x - x^*)^T \frac{\partial^2 f}{\partial x^2} (x - x^*) \\ &= \left(-\frac{1}{2}A^{-1}B^T\right)^T A \left(-\frac{1}{2}A^{-1}B^T\right) + B \left(-\frac{1}{2}A^{-1}B^T\right) + C \\ &\quad + \frac{1}{2}(x + \frac{1}{2}A^{-1}B^T)^T (2A)(x + \frac{1}{2}A^{-1}B^T) \\ &= \frac{1}{4}BA^{-1}B^T - \frac{1}{2}BA^{-1}B^T + C + x^T Ax + \frac{1}{2}Bx + \frac{1}{4}BA^{-1}B^T + \frac{1}{2}x^T B^T \\ &= x^T Ax + Bx + C = f(x)\end{aligned}$$

□

Lemma 1.3.4. Let $p : \mathbb{R}^n \rightarrow \mathbb{R}$ be a PDF given by

$$p(x) = \eta_1 \exp\{-L\}$$

where $L : \mathbb{R}^n \rightarrow \mathbb{R}$, $L(x) = x^T Ax + Bx + C$, and η_1 is a normalizing constant. Then p defines a normal distribution with mean equal to the extremum of L , and covariance matrix equal to $(\frac{\partial^2 L}{\partial x^2})^{-1}$.

Proof. Using Lemma 1.3.3, we know that

$$L(x) = L(a) + \frac{1}{2}(x - x^*)^T \frac{\partial^2 L}{\partial x^2}(x - x^*)$$

where x^* is the extremum of L . Therefore we can rewrite p as

$$\begin{aligned} p(x) &= \eta_1 \exp\left\{-L(a) - \frac{1}{2}(x - x^*)^T \frac{\partial^2 L}{\partial x^2}(x - x^*)\right\} \\ &= \eta_1 \exp\left\{-L(a)\right\} \exp\left\{-\frac{1}{2}(x - x^*)^T \frac{\partial^2 L}{\partial x^2}(x - x^*)\right\} \\ &= \eta_2 \exp\left\{-\frac{1}{2}(x - x^*)^T \frac{\partial^2 L}{\partial x^2}(x - x^*)\right\} \end{aligned}$$

Compare this form of p to the definition of the normal distribution given in Eq. 1.5.

This is just a normal distribution, where $E[X] = x^*$ and $\Sigma^{-1} = \frac{\partial^2 L}{\partial x^2}$. Therefore the mean of p is the extremum of L , and the covariance matrix of p is the inverse of the second derivative of L . □

Lemma 1.3.5. *Inversion Lemma* [probabilisticRobotics]

For $R \in \mathbb{R}^{n \times n}, Q \in \mathbb{R}^{k \times k}, P \in \mathbb{R}^{n \times k}$ where R, Q , and P are all invertible:

$$(R + PQP^T)^{-1} = R^{-1} - R^{-1}P(Q^{-1} + P^T R^{-1} P)^{-1} P^T R^{-1}$$

Proof.

$$\begin{aligned}
& (R^{-1} - R^{-1}P(Q^{-1} + P^T R^{-1}P)^{-1}P^T R^{-1})(R + P Q P^T) \\
&= [\underline{R^{-1}R}] + [R^{-1}P Q P^T] - [R^{-1}P(Q^{-1} + P^T R^{-1}P)^{-1}P^T \underline{R^{-1}R}] \\
&\quad - [R^{-1}P(Q^{-1} + P^T R^{-1}P)^{-1}P^T R^{-1}P Q P^T] \\
&= [I] + [R^{-1}P Q P^T] - [R^{-1}P(Q^{-1} + P^T R^{-1}P)^{-1}P^T] \\
&\quad - [R^{-1}P(Q^{-1} + P^T R^{-1}P)^{-1}P^T R^{-1}P Q P^T] \\
&= I + R^{-1}P[Q P^T - (Q^{-1} + P^T R^{-1}P)^{-1}P^T \\
&\quad - (Q^{-1} + P^T R^{-1}P)^{-1}P^T R^{-1}P Q P^T] \\
&= I + R^{-1}P[Q P^T - (Q^{-1} + P^T R^{-1}P)^{-1}\underline{Q^{-1}Q} P^T \\
&\quad - (Q^{-1} + P^T R^{-1}P)^{-1}P^T R^{-1}P Q P^T] \\
&= I + R^{-1}P[Q P^T - \underline{(Q^{-1} + P^T R^{-1}P)^{-1}(Q^{-1} + P^T R^{-1}P)} Q P^T] \\
&= I + R^{-1}P[\underline{Q P^T} - Q P^T] = I \tag{1.12}
\end{aligned}$$

□

1.3.2 Derivation

Note that in the following mathematical derivation, because $\text{cov}(X, Y) = \text{cov}(Y, X)$, the covariance matrix R_t is symmetric by definition.

We can now begin by rewriting Line 2 of Algorithm 1 (the Bayes Filter) using our

normal PDF definitions (Eq. 1.6 and 1.7):

$$\begin{aligned}
\overline{\text{bel}}(x_t) &= \int p(x_t | x_{t-1}) \text{bel}(x_{t-1}) dx_{t-1} \\
&\approx \det(2\pi R_t)^{-\frac{1}{2}} \det(2\pi \Sigma_{t-1})^{-\frac{1}{2}} \int [\exp\left\{-\frac{1}{2}(x_t - g(\mu_{t-1}) - G_t(x_{t-1} - \mu_{t-1}))^T\right. \\
&\quad \left.* R_t^{-1}(x_t - g(\mu_{t-1}) - G_t(x_{t-1} - \mu_{t-1}))\right\} * \exp\left\{-\frac{1}{2}(x_t - \mu_{t-1})^T \Sigma_{t-1}^{-1}(x_t - \mu_{t-1})\right\} dx_{t-1}] \\
&= \eta \int \exp\{-L_t\} dx_{t-1}
\end{aligned} \tag{1.13}$$

where the determinants are absorbed into a normalizing constant η , and we have defined

$$\begin{aligned}
L_t &= \frac{1}{2}(x_t - g(\mu_{t-1}) - G_t(x_{t-1} - \mu_{t-1}))^T R_t^{-1}(x_t - g(\mu_{t-1}) - G_t(x_{t-1} - \mu_{t-1})) \\
&\quad + \frac{1}{2}(x_t - \mu_{t-1})^T \Sigma_{t-1}^{-1}(x_t - \mu_{t-1})
\end{aligned} \tag{1.14}$$

By assumption, $\overline{\text{bel}}(x_t)$ is a normal distribution. We will define its mean and covariance to be $\bar{\mu}$ and $\bar{\Sigma}$ respectively. In order to compute these matrices, we would like to use Lemma 1.3.4. However, to turn $\overline{\text{bel}}(x_t)$ into the proper form, we will have to get rid of the integral over x_{t-1} . To do so, we will decompose L_t into two terms like so:

$$L_t = L_t(x_{t-1}, x_t) + L_t(x_t) \tag{1.15}$$

where all terms containing x_{t-1} are collected in $L_t(x_{t-1}, x_t)$. This will allow us to move $L_t(x_t)$ outside of $\overline{\text{bel}}(x_t)$'s integral, as it will not depend on x_{t-1} . Then, as long

as we choose our decomposition so that the integral of $L_t(x_{t-1}, x_t)$ equals a constant, we will be left with $\overline{\text{bel}}(x_t)$ in a form where we can apply Lemma 1.3.4.

Now to proceed with this decomposition. Notice that $L_t : \mathbb{R}^n \times \mathbb{R}^n \rightarrow \mathbb{R}$ is quadratic with respect to x_{t-1} . By Lemma 1.3.3 we know that we can rewrite L_t using the extremum with respect to $x_{t-1} : x_{t-1}^*$

$$L_t = \underline{L_t(x_{t-1}^*)} + \frac{1}{2}(x_{t-1} - x_{t-1}^*) \frac{\partial^2 L_t}{\partial x_{t-1}^2} (x_{t-1} - x_{t-1}^*)$$

where the underlined term is L_t evaluated at x_{t-1}^* . This will give us our desired decomposition, turning L_t into the sum of another quadratic expression w.r.t x_{t-1} , and a constant term w.r.t x_{t-1} . Let us now calculate the extremum x_{t-1}^* . To do so, we will first have to find $\frac{\partial L_t}{\partial x_{t-1}}$.

Define

$$\begin{aligned} L_t^1 &= \frac{1}{2}(x_t - g(\mu_{t-1}) - G_t(x_{t-1} - \mu_{t-1}))^T R_t^{-1} (x_t - g(\mu_{t-1}) - G_t(x_{t-1} - \mu_{t-1})) \\ L_t^2 &= \frac{1}{2}(x_t - \mu_{t-1})^T \Sigma_{t-1}^{-1} (x_t - \mu_{t-1}) \end{aligned}$$

then

$$\frac{\partial L_t}{\partial x_{t-1}} = \frac{\partial(L_t^1 + L_t^2)}{\partial x_{t-1}} = \frac{\partial L_t^1}{\partial x_{t-1}} + \frac{\partial L_t^2}{\partial x_{t-1}}$$

and

$$\begin{aligned}
\frac{\partial L_t^1}{\partial x_{t-1}} &= \frac{\partial(x_t - g(\mu_{t-1}) - G_t(x_{t-1} - \mu_{t-1}))}{\partial x_{t-1}} \\
&\ast \frac{\partial L_t^1}{\partial(x_t - g(\mu_{t-1}) - G_t(x_{t-1} - \mu_{t-1}))} && \text{(by Chain Rule)} \\
&= (-G_t^T) \ast \frac{\partial L_t^1}{\partial(x_t - g(\mu_{t-1}) - G_t(x_{t-1} - \mu_{t-1}))} && \text{(by Lemma 1.3.2)} \\
&= -G_t^T R_t^{-1}(x_t - g(\mu_{t-1}) - G_t(x_{t-1} - \mu_{t-1})) && \text{(by Lemma 1.3.1)}
\end{aligned}$$

$$\begin{aligned}
\frac{\partial L_t^2}{\partial x_{t-1}} &= \frac{\partial L_t^2}{\partial(x_{t-1} - \mu_{t-1})} \ast \frac{\partial(x_{t-1} - \mu_{t-1})}{\partial x_{t-1}} = \frac{\partial L_t^2}{\partial(x_{t-1} - \mu_{t-1})} \\
&= \frac{1}{2}(2\Sigma_{t-1}^{-1})(x_{t-1} - \mu_{t-1}) = \Sigma_{t-1}^{-1}(x_{t-1} - \mu_{t-1}) && \text{(by Lemma 1.3.1)}
\end{aligned}$$

which means

$$\frac{\partial L_t}{\partial x_{t-1}} = -G_t^T R_t^{-1}(x_t - g(\mu_{t-1}) - G_t(x_{t-1} - \mu_{t-1})) + \Sigma_{t-1}^{-1}(x_{t-1} - \mu_{t-1})$$

and

$$\begin{aligned}
\frac{\partial^2 L_t}{\partial x_{t-1}^2} &= \frac{\partial(G_t^T R_t^{-1} G_t x_{t-1} + \Sigma_{t-1}^{-1} x_{t-1})}{\partial x_{t-1}} \\
&= (G_t^T R_t^{-1} G_t)^T + (\Sigma_{t-1}^{-1})^T && \text{(by Lemma 1.3.2)} \\
&= G_t^T R_t^{-1} G_t + \Sigma_{t-1}^{-1} \equiv \Phi_t^{-1} && \text{(by covariance matrix symmetry)}
\end{aligned}$$

Now we can compute the extremum:

$$\begin{aligned}
& \frac{\partial L_t}{\partial x_{t-1}} = 0 \\
\implies & (x_{t-1}^* - \mu_{t-1})^T \Sigma_{t-1}^{-1} = (x_t - g(\mu_{t-1}) - G_t(x_{t-1}^* - \mu_{t-1}))^T R_t^{-1} G_t \\
\implies & \Sigma_{t-1}^{-1} (x_{t-1}^* - \mu_{t-1}) = G_t^T R_t^{-1} (x_t - g(\mu_{t-1}) - G_t(x_{t-1}^* - \mu_{t-1})) \\
\implies & \Sigma_{t-1}^{-1} x_{t-1}^* + G_t^T R_t^{-1} G_t x_{t-1}^* = G_t^T R_t^{-1} (x_t - g(\mu_{t-1}) + G_t \mu_{t-1}) + \Sigma_{t-1}^{-1} \mu_{t-1} \\
\implies & \Phi_t^{-1} x_{t-1}^* = G_t^T R_t^{-1} (x_t - g(\mu_{t-1})) + \Phi_t^{-1} \mu_{t-1} \\
\implies & x_{t-1}^* = \Phi_t [G_t^T R_t^{-1} (x_t - g(\mu_{t-1})) + \Phi_t^{-1} \mu_{t-1}] \tag{1.16}
\end{aligned}$$

Thus we can construct our decomposition:

$$\begin{aligned}
L_t(x_{t-1}, x_t) &= \frac{1}{2} (x_{t-1} - x_{t-1}^*)^T \frac{\partial^2 L_t}{\partial x_{t-1}^2} (x_{t-1} - x_{t-1}^*) \\
&= \frac{1}{2} (x_{t-1} - \Phi_t [G_t^T R_t^{-1} (x_t - g(\mu_{t-1})) + \Phi_t^{-1} \mu_{t-1}])^T \\
&\quad * \Phi_t^{-1} (x_{t-1} - \Phi_t [G_t^T R_t^{-1} (x_t - g(\mu_{t-1})) + \Phi_t^{-1} \mu_{t-1}])
\end{aligned}$$

and

$$\begin{aligned}
L_t(x_t) &= L_t - L_t(x_{t-1}, x_t) \\
&= \frac{1}{2}(x_t - g(\mu_{t-1}) - G_t(x_{t-1} - \mu_{t-1}))^T R_t^{-1}(x_t - g(\mu_{t-1}) - G_t(x_{t-1} - \mu_{t-1})) \\
&\quad + \frac{1}{2}(x_t - \mu_t)^T \Sigma_{t-1}^{-1}(x_t - \mu_t) - \frac{1}{2}(x_{t-1} - \Phi_t[G_t^T R_t^{-1}(x_t - g(\mu_{t-1})) + \Phi_t^{-1} \mu_{t-1}])^T \\
&\quad * \Phi_t^{-1}(x_{t-1} - \Phi_t[G_t^T R_t^{-1}(x_t - g(\mu_{t-1})) + \Phi_t^{-1} \mu_{t-1}]) \\
&= \frac{1}{2}(x_t - g(\mu_{t-1}) + G_t \mu_{t-1})^T R_t^{-1}(x_t - g(\mu_{t-1}) + G_t \mu_{t-1}) + \frac{1}{2} \mu_{t-1}^T \Sigma_{t-1}^{-1} \mu_{t-1} \\
&\quad - \frac{1}{2}[G_t^T R_t^{-1}(x_t - g(\mu_{t-1})) + \Phi_t^{-1} \mu_{t-1}]^T \Phi_t[G_t^T R_t^{-1}(x_t - g(\mu_{t-1})) + \Phi_t^{-1} \mu_{t-1}]
\end{aligned} \tag{1.17}$$

Notice that the quadratic and linear x_{t-1} terms cancel out in $L_t(x_t)$. This is to be expected from our decomposition, since $L_t(x_t)$ should be a constant with respect to x_{t-1} . Also, $L_t(x_{t-1}, x_t)$ is the negative of the exponent in a normal distribution, with covariance matrix Φ_t . Because all PDFs integrate to 1, we know:

$$\int \det(2\pi\Phi_t)^{-\frac{1}{2}} \exp\{-L_t(x_{t-1}, x_t)\} dx_{t-1} = 1 \tag{1.18}$$

We now have all the pieces to further simplify $\overline{\text{bel}}(x_t)$:

$$\overline{\text{bel}}(x_t) \approx \eta_1 \int \exp\{-L_t\} dx_{t-1} \quad (\text{by Eq. 1.13})$$

$$= \eta_1 \int \exp\{-L_t(x_{t-1}, x_t) - L_t(x_t)\} dx_{t-1} \quad (\text{by Eq. 1.15})$$

$$= \eta_1 \int \exp\{-L_t(x_{t-1}, x_t)\} \exp\{-L_t(x_t)\} dx_{t-1}$$

$$= \eta_1 \exp\{-L_t(x_t)\} \int \exp\{-L_t(x_{t-1}, x_t)\} dx_{t-1} \quad (\text{by Eq. 1.18})$$

$$= \eta_2 \exp\{-L_t(x_t)\} \quad (1.19)$$

Notice that the $\det(2\pi\Phi_t)^{\frac{1}{2}}$ term was absorbed into the normalizing constant η_2 , since it is a constant with respect to x_t .

Because $L_t(x_t)$ is quadratic, $\overline{\text{bel}}(x_t)$ now satisfies Lemma 1.3.4 (based on Eq. 1.19 and 1.17). So we know that the mean and covariance of the normal distribution representing $\overline{\text{bel}}(x_t)$ will be equal to the extremum of $L_t(x_t)$, and the inverse of its second derivative. We will now compute these values.

$$\begin{aligned}
\frac{\partial L_t(x_t)}{\partial x_t} &= \frac{\partial[\frac{1}{2}x_t^T R_t^{-1} x_t]}{\partial x_t} + \frac{\partial[\frac{1}{2}x_t^T R_t^{-1}(-g(\mu_{t-1}) + G_t \mu_{t-1})]}{\partial x_t} \\
&+ \frac{\partial[\frac{1}{2}(-g(\mu_{t-1}) + G_t \mu_{t-1})R_t^{-1} x_t]}{\partial x_t} + \frac{\partial[-\frac{1}{2}x_t^T R_t^{-1} G_t \Phi_t G_t^T R_t^{-1} x_t]}{\partial x_t} \\
&+ \frac{\partial[-\frac{1}{2}x_t^T R_t^{-1} G_t \Phi_t (-G_t^T R_t^{-1} g_t + \Phi_t^{-1} \mu_{t-1})]}{\partial x_t} + \frac{\partial[-\frac{1}{2}(-G_t^T R_t^{-1} g_t + \Phi_t^{-1} \mu_{t-1})^T \Phi_t G_t^T R_t^{-1} x_t]}{\partial x_t} \\
&= R_t^{-1} x_t - (R_t^{-1} G_t \Phi_t G_t^T R_t^{-1})^T x_t \quad (\text{by Lemma 1.3.1}) \\
&+ R_t^{-1} (-g(\mu_{t-1}) + G_t \mu_{t-1}) \quad (\text{by Lemma 1.3.2}) \\
&- R_t^{-1} G_t \Phi_t (-G_t^T R_t^{-1} g(\mu_{t-1} + \Phi_t^{-1} \mu_{t-1})) \quad (\text{by Lemma 1.3.2}) \\
&= (R_t^{-1} - R_t^{-1} G_t \Phi_t G_t^T R_t^{-1}) x_t \\
&+ R_t^{-1} (-g(\mu_{t-1}) + G_t \mu_{t-1}) - R_t^{-1} G_t \Phi_t (-G_t^T R_t^{-1} g(\mu_{t-1}) + \Phi_t^{-1} \mu_{t-1}) \\
&= (R_t + G_t \Sigma_{t-1} G_t^T)^{-1} x_t \quad (\text{by Lemma 1.3.5}) \\
&+ R_t^{-1} (-g(\mu_{t-1}) + G_t \mu_{t-1}) - R_t^{-1} G_t \Phi_t (-G_t^T R_t^{-1} g(\mu_{t-1}) + \Phi_t^{-1} \mu_{t-1})
\end{aligned}$$

$$\begin{aligned}
\frac{\partial L_t(x_t)}{\partial x_t} &= 0 \\
\implies \bar{\mu}_t &= (R_t + G_t \Sigma_{t-1} G_t^T) [R_t^{-1} G_t \Phi_t (-G_t^T R_t^{-1} g(\mu_{t-1}) + \Phi_t^{-1} \mu_{t-1}) \\
&\quad - R_t^{-1} (-g(\mu_{t-1}) + G_t \mu_{t-1})] \\
&= (R_t + G_t \Sigma_{t-1} G_t^T) [-R_t^{-1} G_t \Phi_t G_t^T R_t^{-1} g(\mu_{t-1}) + R_t^{-1} G_t \mu_{t-1} \\
&\quad + R_t^{-1} g(\mu_{t-1}) - R_t^{-1} G_t \mu_{t-1}] \\
&= (R_t + G_t \Sigma_{t-1} G_t^T) [(R_t^{-1} - R_t^{-1} G_t (G_t^T R_t^{-1} G_t + \Sigma_{t-1}^{-1}) G_t^T R_t^{-1}) g(\mu_{t-1}) \\
&\quad + R_t^{-1} G_t \mu_{t-1} - R_t^{-1} G_t \mu_{t-1}] \\
&= (R_t + G_t \Sigma_{t-1} G_t^T) [(R_t + G_t \Sigma_{t-1} G_t^T)^{-1} g(\mu_{t-1})] \\
&= g(\mu_{t-1})
\end{aligned}$$

$$\begin{aligned}
\frac{\partial^2 L_t(x_t)}{\partial x_t^2} &= \frac{(R_t + G_t \Sigma_{t-1} G_t^T)^{-1} x_t}{\partial x_t^2} \\
&= [(R_t + G_t \Sigma_{t-1} G_t^T)^{-1}]^T = (R_t + G_t \Sigma_{t-1} G_t^T)^{-1} \\
\implies \bar{\Sigma}_t &= R_t + G_t \Sigma_{t-1} G_t^T
\end{aligned}$$

Therefore $\bar{\text{bel}}(x_t) \approx N(x_t; g(\mu_{t-1}), (R_t + G_t \Sigma_t G_t^T))$. So Line 2 of the Bayes Filter, which propagated the belief forward in time based on the state transition PDF, can

be translated into the following two computations:

$$\bar{\mu}_t = g(\mu_{t-1}) \quad \bar{\Sigma}_t = (R_t + G_t \Sigma_{t-1} G_t^T)$$

We are halfway done! The next line of Bayes filter is the update step, which updates the belief distribution based on the most recent sensor measurement:

$$\text{bel}(x_t) = \eta p(z_t | x_t) \bar{\text{bel}}(x_t)$$

As before, let the underlying model of the measurement PDF be given by

$$z_t = h(x_t) + \delta_t$$

where $h : \mathbb{R}^n \rightarrow \mathbb{R}^k$ is an arbitrary function, and δ_t is a random vector of normal distribution with mean 0 and covariance matrix Q_t .

Then we will once again use a first-order Taylor series expansion to approximate h , only now we will expand around our new best estimate of the robot's state: $\bar{\mu}_t$.

$$\begin{aligned} h(x_t) &\approx h(\bar{\mu}_t) + \frac{\partial h(\bar{\mu}_t)}{\partial x_{t-1}}(x_t - \bar{\mu}_t) \\ &= h(\bar{\mu}_t) + H_t(x_t - \bar{\mu}_t) \end{aligned}$$

where

$$H_t = \begin{bmatrix} \frac{\partial h_1(\bar{\mu}_t)}{\partial x_{1_{t-1}}} & \cdots & \frac{\partial h_1(\bar{\mu}_t)}{\partial x_{n_{t-1}}} \\ \vdots & \ddots & \vdots \\ \frac{\partial h_k(\bar{\mu}_t)}{\partial x_{1_{t-1}}} & \cdots & \frac{\partial h_k(\bar{\mu}_t)}{\partial x_{n_{t-1}}} \end{bmatrix}$$

is the Jacobian of h evaluated at $\bar{\mu}_t$.

Then in the same manner as we did with the state transition pdf, we can calculate the mean of the measurement pdf $E[Z]$ to be $h(\bar{\mu}_t) + H_t(x_t - \bar{\mu}_t)$, with covariance matrix Q_t . Thus the measurement pdf has the form

$$p(z_t | x_t) \approx N(z_t; h(\bar{\mu}_t) + H_t(x_t - \bar{\mu}_t), Q_t)$$

Note that just as before, the covariance matrix Q_t is symmetric by definition.

We will begin by rewriting the update step using the normal distribution definitions.

$$\begin{aligned} \text{bel}(x_t) &= \eta_1 p(z_t | x_t) \overline{\text{bel}}(x_t) \\ &\approx \eta_1 \det(2\pi Q_t)^{-\frac{1}{2}} \det(2\pi \bar{\Sigma}_t)^{-\frac{1}{2}} \exp\left\{-\frac{1}{2}(z_t - h(\bar{\mu}_t) - H_t(x_t - \bar{\mu}_t))^T\right. \\ &\quad \left.* Q_t^{-1}(z_t - h(\bar{\mu}_t) - H_t(x_t - \bar{\mu}_t))\right\} * \exp\left\{-\frac{1}{2}(x_t - \bar{\mu}_t)^T \bar{\Sigma}_t^{-1}(x_t - \bar{\mu}_t)\right\} \\ &= \eta_2 \exp\{-J_t\} \end{aligned}$$

where

$$J_t = \frac{1}{2}(z_t - h(\bar{\mu}_t) - H_t(x_t - \bar{\mu}_t))^T Q_t^{-1} (z_t - h(\bar{\mu}_t) - H_t(x_t - \bar{\mu}_t)) + \frac{1}{2}(x_t - \bar{\mu}_t)^T \bar{\Sigma}_t^{-1} (x_t - \bar{\mu}_t)$$

$\text{bel}(x_t)$, as all PDFs, must be normally distributed. We will denote its mean and covariance matrix by μ and Σ . This time there is no integral, and so we can immediately apply Lemma 1.3.4. Therefore the mean and covariance of the normal distribution representing $\text{bel}(x_t)$ will be equal to the extremum of J_t , and the inverse of its second derivative. Let us now compute these values.

$$\begin{aligned} \frac{\partial J_t}{\partial x_t} &= \frac{\partial(\frac{1}{2}x_t^T)}{\partial x_t} - \frac{\partial(\frac{1}{2}x_t^T H_t^T Q_t^{-1} (z_t - h(\bar{\mu}_t) + H_t \bar{\mu}_t))}{\partial x_t} \\ &\quad - \frac{\partial(\frac{1}{2}(z_t - h(\bar{\mu}_t) + H_t \bar{\mu}_t)^T Q_t^{-1} H_t x_t)}{\partial x_t} + \frac{\partial(\frac{1}{2}x_t^T \bar{\Sigma}_t^{-1} x_t)}{\partial x_t} \\ &\quad - \frac{\partial(\frac{1}{2}x_t^T \bar{\Sigma}_t^{-1} \bar{\mu}_t)}{\partial x_t} - \frac{\partial(\frac{1}{2}\bar{\mu}_t^T \bar{\Sigma}_t^{-1} x_t)}{\partial x_t} \\ &= H_t^T Q_t^{-1} H_t x_t - H_t^T Q_t^{-1} (z_t - h(\bar{\mu}_t) + H_t \bar{\mu}_t) \\ &\quad + \bar{\Sigma}_t^{-1} x_t - \bar{\Sigma}_t^{-1} - \bar{\mu}_t \\ &= (H_t^T Q_t^{-1} H_t + \bar{\Sigma}_t^{-1})(x_t - \bar{\mu}_t) + H_t^T Q_t^{-1} (h(\bar{\mu}_t) - z_t) \end{aligned}$$

$$\frac{\partial^2 J_t}{\partial x_t^2} = H_t^T Q_t^{-1} H_t + \bar{\Sigma}_t^{-1}$$

$$\therefore \Sigma_t = (H_t^T Q_t^{-1} H_t + \bar{\Sigma}_t^{-1})^{-1}$$

$$\begin{aligned}
\frac{\partial J_t}{\partial x_t} &= 0 \\
\implies (H_t^T Q_t^{-1} H_t + \bar{\Sigma}_t^{-1})(\mu_t - \bar{\mu}_t) &= H_t^T Q_t^{-1} (z_t - h(\bar{\mu}_t)) \\
\implies \Sigma_t^{-1}(\mu_t - \bar{\mu}_t) &= H_t^T Q_t^{-1} (z_t - h(\bar{\mu}_t)) \\
\implies \mu_t &= \bar{\mu}_t + \Sigma_t H_t^T Q_t^{-1} (z_t - h(\bar{\mu}_t))
\end{aligned}$$

Thus the update step of the Bayes Filter, which incorporated the most recent sensor measurement using the measurement PDF, can be translated into the following two computations:

$$\mu_t = \bar{\mu}_t + \Sigma_t H_t^T Q_t^{-1} (z_t - h(\bar{\mu}_t)) \quad \Sigma_t = (H_t^T Q_t^{-1} H_t + \bar{\Sigma}_t^{-1})^{-1}$$

The only other steps of Bayes' Filter involve normalizing the belief distribution, which we need not perform since we already have the mean and covariance matrix of both $\text{bel}(x_t)$ and $\text{bel}(x_t)$, which are the only pieces of information we need to fully describe their normal distributions. Therefore we can construct a new algorithm, the EKF.

Algorithm 2 Extended Kalman Filter

```

1: function EKF_ITERATE(  $\mu_{t-1}$ ,  $\Sigma_{t-1}$ ,  $z_t$  )
2:    $\bar{\mu}_t = g(\mu_{t-1})$ 
3:    $\bar{\Sigma}_t = (R_t + G_t \Sigma_{t-1} G_t^T)$ 
4:    $\Sigma_t = (H_t^T Q_t^{-1} H_t + \bar{\Sigma}_t^{-1})^{-1}$ 
5:    $\mu_t = \bar{\mu}_t + \Sigma_t H_t^T Q_t^{-1} (z_t - h(\bar{\mu}_t))$ 
6:   return  $(\mu_t, \Sigma_t)$ 
7: end function

```

We could stop here and be done with it. However, the computational complexity of inverting a d by d matrix using today's methods is approximately $O(d^{2.8})$ []. Line 4 of the current algorithm inverts the n by n matrix $\bar{\Sigma}_t$, where n is the dimension of the state vector x_t . So the computation of Σ_t given here is $O(n^{2.8})$. It turns out that we can rewrite Line 4 and avoid inverting the state covariance matrix as so:

$$\begin{aligned}
\Sigma_t &= (H_t^T Q_t^{-1} H_t + \bar{\Sigma}_t^{-1})^{-1} \\
&= \bar{\Sigma}_t - \bar{\Sigma}_t H_t^T (Q_t + H_t \bar{\Sigma}_t H_t^T)^{-1} H_t \bar{\Sigma}_t \\
&= [I - \bar{\Sigma}_t H_t^T (Q_t + H_t \bar{\Sigma}_t H_t^T)^{-1} H_t] \bar{\Sigma}_t \\
&= [I - K_t H_t] \bar{\Sigma}_t
\end{aligned}
\tag{by Lemma 1.3.5}$$

where we make the useful definition

$$K_t = \bar{\Sigma}_t H_t^T (Q_t + H_t \bar{\Sigma}_t H_t^T)^{-1}$$

This shifts the $O(n^{2.8})$ computation of Σ_t to an $O(k^{2.8})$ computation of K_t , where k is the dimension of the measurement vector z_t . Note that in order to keep this new computation of Σ_t at $O(n^2)$, one must multiply matrices in the proper order:

$$\Sigma_t = \bar{\Sigma}_t - K_t (H_t \bar{\Sigma}_t)$$

using the fact that the naive approach to multiplying two matrices of size $n \times m$ and $m \times o$ takes $O(nmo)$ time.

For estimation problems involving state spaces of large dimensionality, n is often much larger than k , and so this change leads to greater computational efficiency, which is important since we would like to run the EKF in real-time.

Lastly, note that

$$\begin{aligned}
K_t &= \bar{\Sigma}_t H_t^T (Q_t + H_t \bar{\Sigma}_t H_t^T)^{-1} = (\Sigma_t \Sigma_t^{-1}) \bar{\Sigma}_t H_t^T (Q_t + H_t \bar{\Sigma}_t H_t^T)^{-1} \\
&= (\Sigma_t (H_t^T Q_t^{-1} H_t + \bar{\Sigma}_t^{-1})) \bar{\Sigma}_t H_t^T (Q_t + H_t \bar{\Sigma}_t H_t^T)^{-1} \quad (\text{by Line 4 of Algorithm 2}) \\
&= \Sigma_t (H_t^T Q_t^{-1} H_t \bar{\Sigma}_t H_t^T + \bar{\Sigma}_t^{-1} \bar{\Sigma}_t H_t^T) (Q_t + H_t \bar{\Sigma}_t H_t^T)^{-1} \\
&= \Sigma_t (H_t^T Q_t^{-1} H_t \bar{\Sigma}_t H_t^T + H_t^T) (Q_t + H_t \bar{\Sigma}_t H_t^T)^{-1} \\
&= \Sigma_t (H_t^T Q_t^{-1} H_t \bar{\Sigma}_t H_t^T + H_t^T Q_t^{-1} Q_t) (Q_t + H_t \bar{\Sigma}_t H_t^T)^{-1} \\
&= \Sigma_t H_t^T Q_t^{-1} (H_t \bar{\Sigma}_t H_t^T + Q_t) (Q_t + H_t \bar{\Sigma}_t H_t^T)^{-1} \\
&= \Sigma_t H_t^T Q_t^{-1} \\
\end{aligned} \tag{1.20}$$

which means the computation of μ_t may also be rewritten using K_t . Thus we can construct our new, more optimal EKF algorithm.

Algorithm 3 Extended Kalman Filter

```

1: function EKF_ITERATE(  $\mu_{t-1}$ ,  $\Sigma_{t-1}$ ,  $z_t$  )
2:    $\bar{\mu}_t = g(\mu_{t-1})$ 
3:    $\bar{\Sigma}_t = (R_t + G_t \Sigma_{t-1} G_t^T)$ 
4:    $K_t = \bar{\Sigma}_t H_t^T (Q_t + H_t \bar{\Sigma}_t H_t^T)^{-1}$ 
5:    $\Sigma_t = (I - K_t H_t) \bar{\Sigma}_t$ 
6:    $\mu_t = \bar{\mu}_t + K_t(z_t - h(\bar{\mu}_t))$ 
7:   return  $(\mu_t, \Sigma_t)$ 
8: end function

```

1.3.3 Remarks

In total the EKF algorithm has a computational complexity of $\max(O(n^{2.8}), O(k^{2.8}), O(g), O(h))$ per iteration, where the complexity of executing the functions g and h is unknown, but in practice are often $O(1)$.

Chapter 2

Hardware

Now that we have covered the necessary mathematical background of the main algorithm used in this thesis, we will move on to an overview of the rover's design.

2.1 Specific Hardware Used

The hardware used in this project was chosen to minimize cost while producing a vehicle capable of navigating rough outdoors terrain. Parts that were already on hand, and that most college students would reasonably have access to, such as a personal laptop and an Android smartphone, were used over superior alternatives. In total these parts were purchased for less than \$500, with most of that cost coming from the rover's base rather than its sensors.

The mobile base chosen was the Lynxmotion A4WD1 Rover, shown in Figure 2-1. It was purchased as a kit including four 200 RPM DC gear motors, four 100 PPR motor encoders, and four 4.75" diameter wheels. The motor encoders are sensors

which measure the rotation of the motors, and thus of the wheels. The chassis consists of four aluminum side brackets, and polycarbonate top and bottom panels. This kit made up the bulk of the rover's cost. It was chosen for its large wheels and strong motors, increasing the rover's robustness to uneven terrain and ramps. The chassis can support up to 5 lbs overall, and a second stackable level is available as an extension. While not purchased, this second level would be an ideal place to put a tablet or small laptop.

One downside of this base is the fixed position of the four wheels. The lack of a turnable axis means the rover must

Figure 2-1:
[fig_lynxmotion_rover]

steer by varying the speed of its motors. This causes wheel slippage in one or more of the wheels when the rover turns, meaning the motor encoders do not see the distance traveled.

This ultimately causes greater error buildup in the robot's localization. Choosing a different base which only uses two wheels would avoid this issue, and likely be cheaper. However, such a choice must be balanced with the robot's suitability for outdoor use, and room for all on-board components.



The motors are controlled by a Sabertooth 12A 6V-24V regenerative motor driver. There is a 5A version of this motor driver, which should have been purchased to save \$20. This driver is dual-channeled, i.e. it controls two separate motor channels. Two DC motors are attached to each channel, so that the left and right side wheels of the rover are each controlled by a single channel. The Sabertooth drives DC motors from these channels in a relatively simple way. The speed of DC motors is proportional to

the voltage supplied to them, and the direction of rotation can be flipped simply by flipping the polarity of the supplied voltage. So the motor driver manages speed by modifying the voltage supplied to each channel. To do so it uses a technique called pulse-width modulation, which involves switching the power on and off at a high frequency. This approximates a smooth waveform of the average voltage and current. To change the direction of rotation, an on-board circuit called the H-bridge is used to flip the polarity of voltage supplied. [**dcMotorBlog**]

The motor driver is powered by two LG 18650 HE2 rechargeable lithium ion cells, which sit in a battery case. This case was made out of an 18650 battery holder soldered in series to act as a pack. The battery cells were individually charged before each use by a NiteCore-i2-V2014 li-ion charger. The Sabertooth motor driver has built-in lithium ion over-discharge protection, which ensures that the cells will not be discharged beyond their maximum capacity.

Figure 2-2: Situated on top of the rover is the PING))) ultrasonic distance sensor (see Figure 2-2), which is attached to a Parallax



servo which pans back and forth 180 degrees. This range sensor emits an ultrasonic chirp, and times how long it takes for that chirp to echo back. Based on that time, the distance from the sensor to an obstacle can be calculated. The PING))) sensor can be used to detect objects from 2cm to 3 meters away.

[**pingDocumentation**]

At the heart of the rover is an Arduino Uno R3, shown in Figure 2-3. This microcontroller board handles low level control of the rover. It is hooked up to every

other electronic on the rover by its input and output pins. It commands the motor driver, telling it at what speed to set the two output channels, and directly controls the panning motion of the Parallax servo. It also transmits sensor measurements to the computer. It is connected to this computer via a USB cable, which powers the board and allows communication over a serial port. Motor encoder values and ultrasonic range data are transmitted, and motor speed commands are received. An Arduino prototyping shield was stacked on top for soldering connections, to allow re-usability of the board.

Only two of the four available motor encoders are used, due to a limit of the microcontroller board used. Choosing a different model with more hardware interrupt pins would improve localization accuracy, without drastically increasing the price.

Figure 2-3:
[fig_arduino_uno]



The computer used is a Dell Inspiron 3531 laptop, which has a quad-core 2.16 GHz processor, and 4 GB of RAM. Any personal laptop running Ubuntu or Debian could be used here, and additional computational resources would be beneficial. However, this laptop was a personal work machine and already available to use at no additional cost. The laptop is used as the main processing unit.

The last component in the design is a Nexus 4 smartphone placed on top of the rover, behind the ultrasonic sensor. Just like the Arduino board, it is connected to the laptop by USB. Inside this phone is an MPU-6050 chip which contains a digital gyroscope and accelerometer. Elsewhere on the phone's logic board is a magnetometer,

otherwise known as a digital compass, and a GPS receiver. This was also a personal device already available, which acts as a cheap Inertial Measurement Unit (IMU) and GPS receiver for the robot.

Both USB cables used are just under 10 feet long. The USB 2.0 specification limits the length of cable between two 2.0 USB devices to less than five meters, or about 16 feet [[usbForum](#)]. Thus there should be no connectivity problems given the current length, but the cables cannot be extended much further.

Connecting electronics on the rover to the laptop via USB means the processing laptop must be manually kept within 10 feet of the rover as it navigates. Thus the rover is not truly autonomous. It could be made so by including wireless or radio communication with a server, or by using a larger chassis which would be able to simply carry the laptop. However, USB cables are cheap, and the current design still functions as a proof of concept for an autonomous rover.

2.2 Construction

Figure 2-4 shows the base just after assembly. The aluminum side brackets' mounting holes did not line up properly with the motors, so a Dremel drill was used to widen them.

Figure 2-4: Constructed Chassis

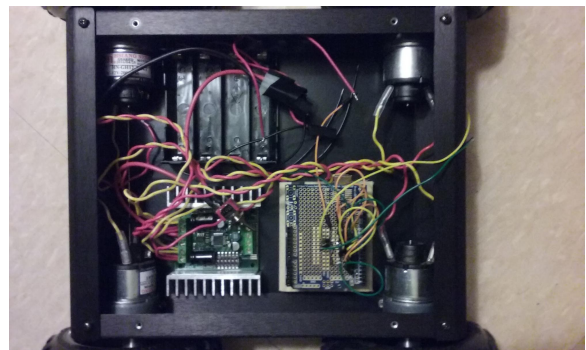


The Arduino Uno was screwed to a 2.5" x 3" x 0.5" wooden poplar block, with non-conductive nylon washers placed between the screw head and the Uno, and between the Uno and the wooden block. The wooden Arduino mounting board and the motor driver were both attached via double-sided foam mounting tape to the bottom panel of the rover. The battery holder was attached with glue dots for easier removal.

The servo fits conveniently into a pre-cut opening in the top chassis panel, and is held in place with four 3mm x 6mm screws and corresponding washers. A mounting bracket is attached to the servo, and the PING))) sensor is screwed to that mounting bracket, using non-conductive washers and screws to separate the circuit board and the metal mounting bracket.

Another opening in the top panel allows the PING))) sensor to connect to the Ar-

Figure 2-5: Pieces Mounted



duino inside the body of the rover. This opening also allows the USB cable connected to the Arduino to reach the laptop. The smartphone sits on the top panel just to the left of this opening, secured in place by removable glue adhesive dots. It is also connected to the laptop via a micro-USB to USB cable.

Figure 2-6: Construction Finished



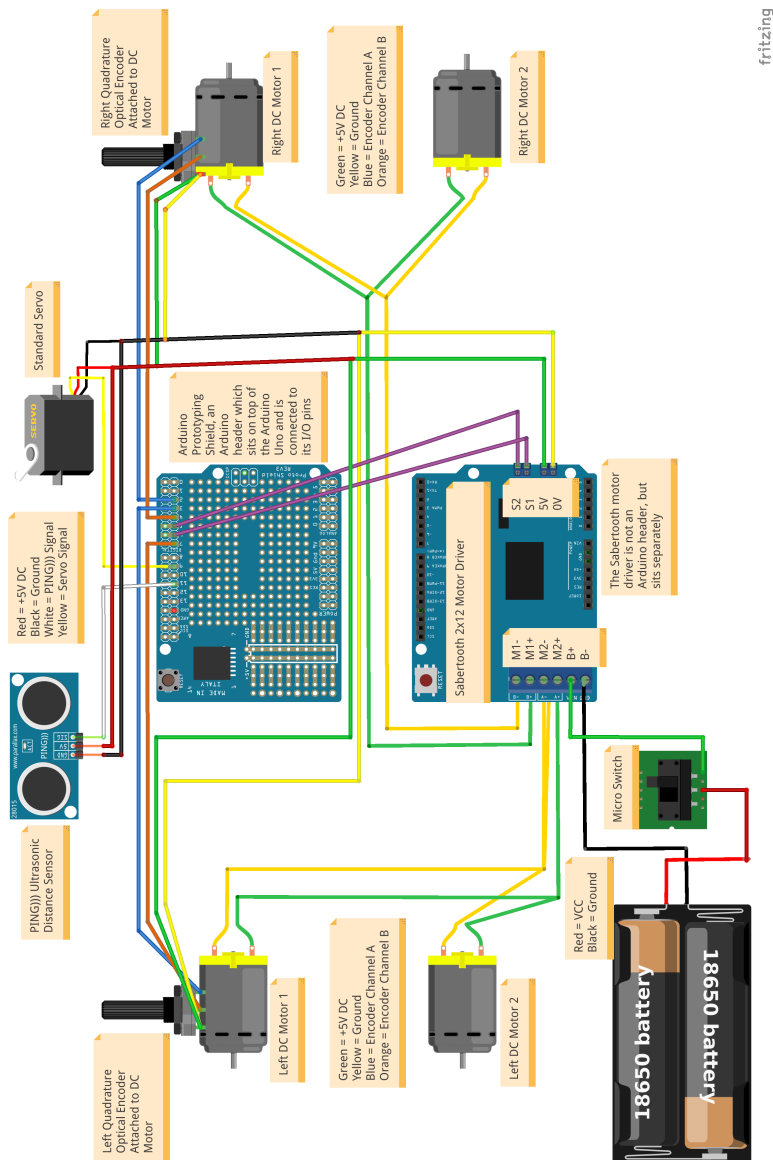
For the configuration of electrical connections between parts, see Figure 2-7. These connections were made with flexible stranded core, 22 AWG breadboard wire. Connections to the Arduino's digital pins were made indirectly. A prototyping shield was stacked on top of the Arduino, and connected to its digital pins via pin headers. Signal pins were then soldered to the prototyping shield. Breadboard wires needing direct connection ideally should use terminal block connectors. However, these were difficult to find at a reasonable price, and so wires were soldered together tip to tip, and simply wrapped in electrical tape.

2.3 Power

Refer once more to Figure 2-7 for a visual depiction of the power connections described here.

Besides the Arduino Uno, which is powered separately by a USB connection to the laptop, most of the rover's components are powered through the battery pack.

Figure 2-7: Electrical Connections



This image was created with Fritzing

This pack contains two individual 18650 lithium-ion cells connected in series. The battery pack is then connected to the motor driver's battery terminals B+ and B-. The positive B+ output goes through a microswitch, which is attached to one of the rover's side brackets, and is accessible from the outside. This acts as a kill switch for the battery pack.

The battery pack powers the motor driver, and excess power is then routed through the Sabertooth's on-board battery eliminator circuit (BEC). The BEC efficiently regulates the incoming voltage down to 5V, which is what the other electronics expect. The BEC outputs are labeled 0V and 5V in Figure 2-7. The ultrasonic sensor, its servo, and the two motor encoders are all powered through this BEC. The Arduino is also connected to this BEC's ground, as the microcontroller and motor driver must share a common ground plane in order for control signals to be correctly interpreted [**sabertoothUserGuide**]. It is important to note that a BEC of some kind is essential in this project, as the Arduino's on-board 5V regulator can not handle the peak amperage draw of the servo.

Lithium ion cells hold 4.2V at full charge, and discharge down to a minimum of 2.7V. The Sabertooth has a lithium cutoff mode which senses the average voltage of cells in the battery pack, and shuts the driver down when that average dips below 3.0V. Cells connected in series add their voltage, so the voltage supplied through the motor driver's output channels will range from 8.4V to 6.0V, which is within the acceptable operating range for the DC motors. The specific li-ion cells being used can supply up to 20A continuously, and the motor driver can handle up to 12A per channel. The motors each draw a maximum current of 1.5A, and two are used per

channel, putting the total possible current draw at 3A per channel, well below the limits of the motor driver and battery pack.

The BEC supplying power to the sensors is capable of supplying up to 1 Amp of continuous current, and 1.5 Amps of peak current. The ultrasonic sensor and the two motor encoders combined use less than 500 mA. However the standard servo - while normally drawing less than 500 mA itself - has the potential to draw peak currents of up to 1A if it hits a snag and is stopped from moving. The sensors are therefore pushing the limits of the BEC's operating range. It is also important to check that the wires connected to the BEC are capable of handling the peak current without burning out. 22 AWG wires with 43 or more internal cores are rated to handle up to 1A of current. The rover's 22 AWG breadboard wires have a bit less than 43 internal cores, but have yet to have any issues. But the servo has not been under full load by being stopped, and so the wires have not truly been tested. Ideally those replicating this construction will use larger wires rated for higher current, to be safe.

Note that when using the rover, the sensors attached to the Arduino should be powered off first, else the Arduino may try to power itself via its input pins. The sensors are powered from the BEC on the motor driver, so they may be turned off by flipping the microswitch between the battery pack and motor driver.

Chapter 3

Arduino

The rover's Arduino Uno acts as a bridge between hardware and software, allowing the laptop to read sensor data from the rover, and control the speed of its wheels.

3.1 Background

Arduino development boards are printed circuit boards capable of running small embedded programs. They contain an on-board microcontroller, timing crystal, USB port, I/O pins and more. The specific board used in this project, an Arduino Uno, uses the ATmega328P microcontroller with a 16 MHz quartz timing crystal and 14 digital I/O pins. It also has 6 analog-to-digital converter I/O pins, but we will not make use of them in this project.

Digital I/O pins can be configured to either read signals as input or generate them as output. Digital pins read input signals as binary values, i.e. the signal's voltage is considered either HIGH or LOW compared to a certain threshold voltage. When

digital pins are configured to generate HIGH or LOW signals, they produce a relative output voltage above or below the threshold voltage.

3.1.1 Servo Control Pulses

An important use-case which pops up often when using the Arduino is that of interfacing with RC electronics. In this project's design, both the Sabertooth motor driver and the standard servo require their signal inputs to use the standard R/C transmission protocol.

This protocol involves sending brief HIGH pulses of variable width, between one and two milliseconds long. There is a fixed delay between these pulses: usually about 20 ms of LOW signal. The width of the HIGH pulse communicates to a servo the desired position. Its internal components then drive its DC motors until the servo is rotated to the commanded position. In the case of the Sabertooth motor driver, the position is interpreted as the speed at which to drive the motors.

3.2 Arduino Uno Connections

Refer back to Figure 2-7 for a visual representation of how the Arduino Uno is connected to the other rover components.

3.2.1 Hardware Interrupt Pins

As one can see in Figure 2-7, only two motor encoders are used: the ones attached to the rover's front-left and front-right wheels. This is due to a hardware limitation

of the Arduino Uno. The ATmega328P microcontroller has only two interrupt pins, which are mapped to digital pins 2 and 3 on the Uno. These pins can trigger unique Interrupt Service Routines (ISRs) whenever the input signals change from LOW to HIGH voltage, or vice versa.

While it is possible to react to a change in any digital pin's voltage, it would be significantly slower than a hardware interrupt. An ISR is necessary to keep up with the fast rate of pin voltage changes that occur in the motor encoder output.

If a different Arduino board such as the Mega were used, there would be sufficient hardware interrupt pins for all four encoders. Using a board with plentiful interrupts, one could even attach both channel outputs of the encoders to interrupt pins, rather than only one. This would double the encoders' resolution, as will be explained in section 3.4.3.

3.2.2 Digital Pin Connections

Each motor encoder has two output channels, A and B. Both encoders attach one of their output channels, channel A, to a hardware interrupt pin. In section 3.4.3 we will see why this configuration was chosen. The right motor's encoder connects channel A to pin 2, and channel B to pin 4. The left motor's encoder connects its channel A output to pin 3, and its channel B output to pin 7.

The S1 and S2 signal input terminals on the Sabertooth motor driver are connected to pins 5 and 6. The control signal for the hobby servo is connected to pin 9, while the signal pin on the ultrasonic sensor is connected to pin 11. The Arduino's ground pin

is connected to the ground of the motor driver's BEC, to ensure a common ground plane.

Most digital pin numbers used are arbitrary, and connections may be permuted without issue. The exceptions are pins 0-3, which must not be modified. Pins 0 and 1 must be left unattached for serial data transfer to work properly over USB. And pins 2 and 3 are hardware interrupt pins which must be used to handle the motor encoders' output.

3.3 Motor Driver's Configuration

The Sabertooth motor driver has two signal input terminals, S1 and S2, which allow the Arduino to issue instructions specifying how to drive the motors. The protocols used to communicate with the motor driver over these signal inputs are specified by six DIP switches on-board the driver. These DIP switches are manually flipped either up or down.

Setting switch 1 down and switch 2 up places the driver into R/C input mode, which configures S1 and S2 to expect servo control pulses à la R/C controllers. This protocol was briefly explained in section 3.1.1. Turning switch 3 down selects the lithium cutoff mode, which detects the number of lithium cells in series powering the driver, and shuts off when the battery pack's voltage drops below 3.0V per cell. This prevents accidental damage to the 18650 cells from over-discharge. Flipping switch 4 down selects independent (differential) drive, which allows S1 and S2 to each independently control the speed of one motor channel. Using this mode, turning off

the vehicle is achieved by lowering the relative speed of the motors on one side of the vehicle compared to the other.

Switch 5 is flipped up to ensure a linear rather than exponential response of the motors to the Arduino's input signal. Switch 6 is flipped down to select "microcontroller mode", which turns off auto-calibration of the zero-velocity input signal, and turns off an automatic timeout. Thus if the signal connection is somehow lost the motor driver will continue driving the motors according to the last signal received. This is necessary for smooth performance of the motors since the Arduino may slightly delay control pulses. Note that this does introduce the risk of a runaway rover should electrical wiring become disconnected.

3.4 Arduino Sketch

A sketch is Arduino-speak for an embedded program written for an Arduino board. There is an Arduino IDE which supports development of sketches in C or C++, and allows one to take advantage of a software library for common I/O interactions. After the code is written in this IDE, it is uploaded to the board over a USB serial connection. The board will then continuously execute the code found in the sketch's main loop as long as the board is powered. This embedded software interacts with the rover's various sensors and other electronics on a low level, through reading from and writing to the Arduino's digital I/O pins.

One of the standard Arduino libraries is the Servo library. This library allows one to configure a digital pin to output RC control pulses, as explained in section 3.1.1.

The sketch used in this project makes use of this library to set the speed of the two sets of wheels controlled by the Sabertooth motor driver, and also to set the position of the standard servo. The motor driver is sent HIGH pulses every 20 ms, of length one to two ms. The standard servo is also sent HIGH pulses every 20 ms, but these pulses vary from 0.75 to 2.25 ms, as specified by its datasheet.

3.4.1 Ultrasonic Sensor

The PING))) ultrasonic distance sensor works by emitting a short burst of 40 kHz sound waves and timing the delay before an echo response. The Arduino triggers a ping by generating a brief $5 \mu\text{s}$ (microsecond) pulse on the sensor's bi-directional signal pin. The sensor then generates a HIGH output pulse, which continues until either the echo is received or the maximum amount of time - 18.5 ms - has passed. The response time is then multiplied by the speed of sound in air, to calculate an estimated distance to the first object in front of the sensor. [[pingDocumentation](#)]

The rover's sketch uses the NewPing library to handle this protocol [[newPing](#)]. This library provides a convenient method, ping(), which returns the echo time in μs . The sketch avoids costly floating point computations by sending this echo time directly to the laptop, rather than computing the distance on the Arduino board.

3.4.2 Servo

The ultrasonic sensor can only detect objects in front of it within roughly 5-20deg [[pingDocumentation](#)]. Thus for the rover to have a better approximation of its

surroundings, the sensor needs to be panned back and forth. This is what the standard servo it is attached to allows. The sketch makes use of the Servo library to control the servo with R/C pulses. An angular degree from 0 to 180 is written to a Servo object, and the Servo library handles generating the output signal corresponding to that degree on the appropriate pin.

The sketch sweeps the servo back and forth one degree at a time, and at each step an ultrasonic ping is emitted, the echo time for that ping is measured, and the most recent measurements from all sensors are published. This means that the delay between servo steps defines the publishing frequency of sensor data on the Arduino. This delay is currently set to 100 ms, which corresponds to a 10 Hz publishing frequency. The frequency could be increased, but a bare minimum delay of 30 ms is necessary to give the servo time to finish moving, and the PING))) sensor time to recover and prepare for the next ping.

The basic idea is shown in the following code fragment:

```
while (servoPos < SERVO_LEFT) {  
    sonicServo.write(servoPos); // Set servo position  
    timer = millis(); // current time in ms  
  
    while (millis() - timer < SERVO_STEP_DELAY) {  
        nh.spinOnce(); // handle callbacks  
    }  
  
    ping_time_uS = sonar.ping(); // Get echo time
```

```
    publishSensorMessages(servoPos, ping_time_uS);

    servoPos++;
}

}
```

This code is executed inside the sketch's main loop, and a similar while-loop is run right after, which decrements the servo position back to SERVO_RIGHT. `millis()` is an Arduino built-in function which uses a hardware timer to count how many milliseconds have passed since the board was turned on. The callback handling that occurs while waiting reads the incoming serial buffer for any data, and if motor commands are found, executes an appropriate callback function. `publishSensorMessages()` sends over serial the ultrasonic echo time, the servo's current angle, and the tick count of both encoders (see next section). Section 4.2 will describe how this data is passed between the laptop and Arduino.

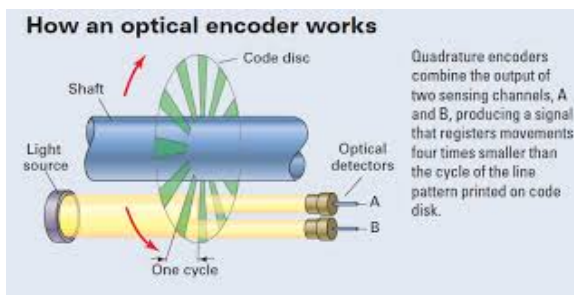
3.4.3 Quadrature Encoders

An important function of the Arduino sketch is to track the movement of the motors. Our system may command the motor driver to move the rover's wheels with a certain fraction of the maximum available power, but it is difficult to predict with precision the resulting angular velocity. For one thing, the RPM of DC motors is proportional to the supplied voltage. But the voltage supplied to the motors through the motor driver is coming from an external li-po battery pack, which generates variable voltage. It starts at 8.4V and drops to a minimum of 6.0V before the motor driver shuts off. Thus even if the same servo control pulse is continuously sent to the motor driver,

the motors' angular velocity will decrease over time.

In order to measure the angular velocity of the motors, motor encoders are attached. These feedback devices are incremental position encoders, meaning they monitor the change in the motor shaft's position compared to its starting position.

Figure 3-1: [fig_optical_encoders]



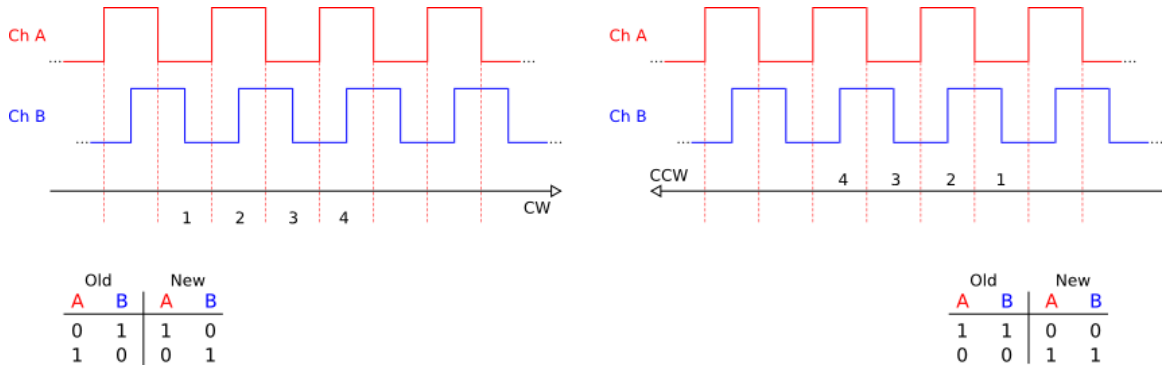
The motor encoders which came with the Lynxmotion rover kit are optical quadrature encoders. This type of encoder attaches a flat disk with thin slits known as the code disk to the motor's gear shaft. Two photodiodes, components which transform light into electric current, are placed above the disk side by side. A light source shines light through the disk from the other side. Figure 3-1 gives a visual illustration.

As the motor spins the gear shaft, the code disk turns with it. This produces an on-off pattern of light on the photodiodes, which produce two square waves as signal outputs. These two channels of output pulses are referred to as channels A and B. Depending on the direction of rotation, channel A's square wave will either lag behind or be ahead of channel B. This can be seen in Figure 3-2 which shows example output pulses as a motor turns clockwise (CW) or counter-clockwise (CCW). [encoderBlog]

The number of slits in the code disk corresponds directly to how many pulses each channel will produce in one revolution of the DC motor. This parameter is known as the pulses per revolution (PPR), and is given by the manufacturer. By counting how many pulses occur per second, and using the PPR, one can calculate the angular

velocity of the motor. At maximum resolution, one can watch each square wave for a change in voltage from LOW to HIGH or HIGH to LOW. This gives a maximum resolution of $4 * PPR$ detectable position increments per revolution.

Figure 3-2: [encoderBlog]



Handling rapid changes in voltage is exactly what hardware interrupts are designed for. Unfortunately, for maximum resolution each encoder needs two hardware interrupt pins, one for each output channel. The Arduino Uno only has two hardware interrupt pins, and our rover has two sides. It would be nice if we could at least use two encoders, one for each side.

We achieve this by reacting to changes in voltage in only one channel per encoder. In the two tables in Figure 3-2, LOW voltage values are encoded as 0, and HIGH voltage values as 1. The first plot in the figure shows the output of the two channels when the motor is moving in the CW direction. Assume we only watch for transitions on channel A. When channel A transitions from the section labeled 1 to section 2, it is rising from 0 to 1, and channel B has value 0. That information alone tells us that the motor's gear shaft is turning, but not in what direction. However, at the next transition between sections 2 and 3, channel A falls from 1 to 0, and channel

B has value 1. Now we are confident that channel B began its pulse after channel A. This means that the photodiode generating channel B detected light after channel A's photodiode, i.e. the code disk is turning in the direction of photodiode A to B. Datasheet specifications will tell us that this translates to the CW direction. It turns out that for each channel A transition event, the previous and current channel values are sufficient to uniquely determine the direction of rotation of the motor. Thus, while only monitoring one of the channels lowers our resolution to $2 * PPR$ counts per revolution, it allows us to use hardware interrupts for two quadrature encoders rather than only one. [[encoderBlog](#)]

The sketch uses an implementation described in [[encoderBlog](#)], which creates a lookup table using the four binary digits representing the previous and current channel states. These digits form a four-bit binary number, which indexes into a sixteen element array. Each element of this array stores either 1, -1, or 0, where 1 represents a movement in the CW direction, -1 represents a movement in the CCW direction, and 0 represents an undetermined transition. This lookup table is then used by the sketch when it reacts to a hardware interrupt caused by the channel A output of one of the encoders. When this interrupt occurs, the code reads the values of channels A and B from the corresponding digital pins, and combines them with the previous values to find the appropriate index in the lookup table. The value at that index is then added to a global counter variable, which keeps track of the net number of incremental movements from the motor's starting position. A net negative number indicates how far the motor has rotated in the CCW direction since it started, and a net positive number indicates how far the motor has rotated in the CW direction.

[encoderBlog]

The implementation described above is shown in the following code fragment which defines the Interrupt Service Routine (ISR) that handles encoder events for the front-left encoder. [encoderBlog]

```
volatile long encLeftCount = 0L;

const int8_t encoder_lookup_table[] =
{ 0,0,0,-1,0,0,1,0,0,1,0,-1,0,0,0 };

void encoderLeft_isr() {
    static uint8_t encLeft_val = 0;
    encLeft_val = encLeft_val << 2;
    encLeft_val = encLeft_val |
        ( ((PIND & 0b100) >> 1) |
        ((PIND & 0b10000) >> 4) );
    encLeftCount = encLeftCount +
        encoder_lookup_table[encLeft_val & 0b1111];
}
```

When the digital pin connected to the encoder's Channel A output changes, the main loop of the sketch is interrupted and this ISR is executed. Until this ISR finishes, no other code is run, including other ISRs, although they may be flagged for future execution. Therefore ISRs must be as fast as possible, to ensure that no interrupt events are dropped and that the main loop continues running smoothly.

To this end, this ISR makes use of constants and low-level C and avr microcontroller commands to ensure a speedy execution, at the price of readability. PIND is an avr command which returns input readings from digital pins 0-7 encoded into a byte. Bit shifting and masking are then used to extract and store the values of pins 2 (channel A) and 4 (channel B) into the two least significant bits of the encLeft_val variable. This variable is static, and so retains its value between ISR executions. The count is then incremented according to the lookup table.

When the sketch's main loop publishes sensor readings, it needs to publish the current encoder tick count for the right and left encoders. However, reading from multi-byte variables which are accessed within and without an ISR risks data corruption in the event that the ISR interrupts the main thread in-between byte reads. Since the encoder tick count variables are four bytes long, interrupt guards must be used around a read to make it atomic. These guards temporarily stop the custom ISR from executing while the global variables are copied over to local ones. This is shown for the left encoder count in the following snippet from the sketch:

```
detachInterrupt(digitalPinToInterrupt(encLeftAPin));  
  
encMsg.leftTicks = encLeftCount;  
  
attachInterrupt(digitalPinToInterrupt(encLeftAPin),  
    encoderLeft_isr, CHANGE);  
  
t = 0;
```

Similar guards are used for the right encoder count variable.

Because we are turning interrupts off briefly, there is the risk that we could miss an interrupt event on one of the channel A pins. Missing an edge pulse from one of the encoders would not only lose that tick, but would also throw off the next value we index into the lookup table. Luckily, the Arduino has a single-bit interrupt event flag for every interrupt event. Therefore even in the worst case scenario, where an encoder interrupt event occurs just after the ISR is turned off, that event is flagged. As long as the ISR is re-enabled and handles that flag before a second interrupt event occurs, there will be no problem. After re-enabling the ISR, the next program instruction is guaranteed to be executed before handling any flagged events. To ensure speedy handling of a flagged event, a meaningless instruction is executed which assigns zero to the local variable t .

Let us calculate how often each interrupt event occurs. Each encoder generates 100 pulses per revolution. We will only be watching one of the square waves (output channel A), so there will be 200 edge transitions per revolution. The motors have a maximum speed of 200 RPM, so each encoder is guaranteed to revolve less than 3.4 times per second. Thus there will be at most

$$3.4 \text{ rev/sec} * 200 \text{ events/rev} = 680 \text{ events/sec}$$

And we are guaranteed to have at least $1/680 \approx 1.4$ ms between encoder interrupt events.

So the code inside the interrupt guards needs to take significantly less than 1.4 ms to execute, in order to allow a flagged interrupt event to be handled before the

next event occurs. Each global encoder count variable is four bytes, so assignment compiles to four machine instructions. The assignment of zero to the one-byte variable `t` takes one machine instruction. The helper macro `digitalPinToInterruption()` is a preprocessor `#define`, and so takes zero machine instructions. Therefore there are five total machine instructions executed inside the interrupt guards. The Uno uses a 16 MHz quartz timing crystal, so executing one instruction takes

$$1/(16000000 \text{ } Hz) = 62.5 \text{ nanoseconds}$$

Thus to run the five instructions takes $5 * 62.5 \text{ ns} = 0.3125 \mu\text{s}$. After that is finished, the flagged event must be handled. External interrupt calling has an overhead of $5.125 \mu\text{s}$, just to enter and leave the function [`gammonInterrupts`]. Thus as long as the ISR executes in less than $1.4 \text{ ms} - 0.0003125 \text{ ms} - 0.005125 \text{ ms} = 1.3945625 \text{ ms}$, the sketch will never miss an encoder event. Testing of the ISR indicates that this is an order of magnitude more time than needed.

Chapter 4

ROS

The software system controlling the rover and processing the incoming sensor data is built on top of the Robot Operating System (ROS). ROS is a meta operating system for open-source robotics. It provides an asynchronous messaging framework for multiple processes to communicate across multiple machines, package management for shared robotics libraries, and makes it easy to handle multiple moving coordinate systems.

4.1 ROS Basics

4.1.1 Messaging

Processes in ROS are known as nodes. Nodes communicate by publishing and subscribing to certain communication channels called topics. The data passed over these topics are various classes of rigidly defined data structures called messages. Messages often contain meta-data such as a timestamp and sequence number, in addition to

the data of interest.

When a node publishes a message to a particular topic, all nodes subscribed to that topic receive a copy. Any number of processes may publish or subscribe to a topic, making this a many-to-many communication protocol. Under the hood, messaging between nodes is handled by the ROS Master node, which acts like a DNS server and must be running for the ROS system to function.

We will use a simple example to illustrate. Assume a fresh ROS system, with only two nodes: A and B. If node A wishes to subscribe to messages coming from topic "/foo", it will register its intent with the Master. Then, if node B starts publishing messages to topic "/foo", it will also register this with the Master. When node B does so, the Master node will notify all registered subscribers on the "/foo" topic. Node A will receive the TCP/IP socket address of Node B, and communicate directly to negotiate opening a socket. Then each time node B publishes a message to "/foo", it will iterate through its list of connected sockets nodes, and push message data through each one. Every time the list of registered subscribers or publishers for topic "/foo" is updated, the Master node notifies all nodes registered to that topic.

4.1.2 Packages

Packages are collections of related ROS resources which all work together to perform some specific task. They often include source code for nodes, executable utilities, message definitions, and launch files. There are also meta-packages which collect various related packages.

Launch files are XML files which define several nodes to be run at once. Robotics systems grow large quickly, and require many nodes. This project ended up using 12 nodes throughout its launch files. Manually starting all of those nodes would be tedious, and launch files automate that process. They also allow convenient parameter specification for each node. Parameters are stored in separate files, and are loaded dynamically when a launch file is run.

4.1.3 Frames and Transforms

Robotics systems include many moving parts. In order to keep track of those parts and their relation to one another, many different coordinate axes are needed. In ROS, these coordinate axes are called frames, and just like topics they are each given a unique name. The rover works with five frames in total, and follows the standards specified in REP-103 and REP-103 [REP-103] [REP-105].

The basic starting frame is the "base_link" frame, which has its origin at the center of the rover. This frame is rigidly attached, and follows the translation and rotation of the rover. The X axis of the base_link frame always points forward, the Y axis points to the robot's left, and the Z axis points straight up above the robot.

Next we define a frame for the smartphone, simply called phone. The phone frame has its origin at the center of the phone, roughly two inches to the right of the base_link frame. This frame is once again attached, and moves with the translation of the smartphone. However, while the origin shifts, the orientation of the axes stays constant with respect to the earth. The X axis always points east, its Y axis points

north, and its Z axis points up towards the sky, or tangential to the earth's surface.

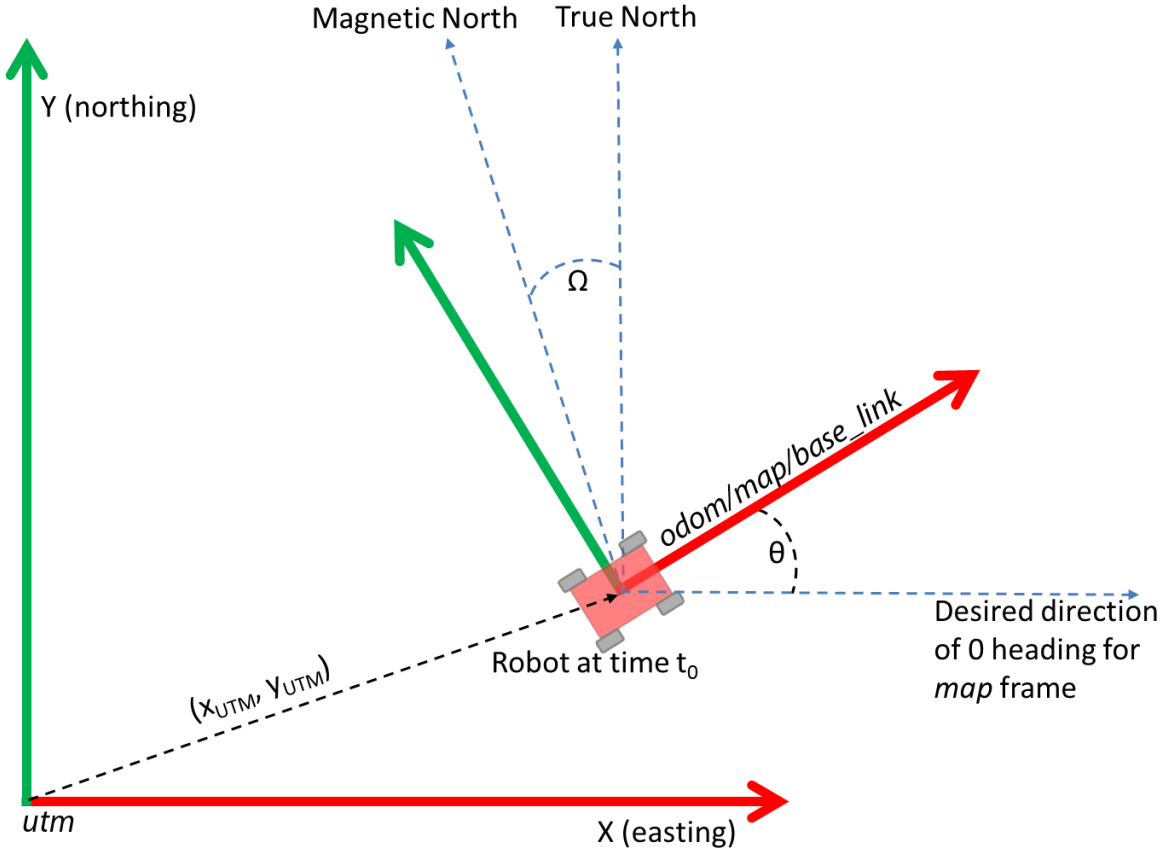
This axis orientation is referred to as the ENU convention (East-North-Up).

Another frame needed is a frame fixed to the local environment. The origin and orientation of this frame should be the same as the `base_link` frame initially: origin at the center, X axis forward, Y to the left, and Z up. However, this frame will not be rigidly attached to the rover body, and will not move or rotate as the rover moves. Thus it will be able to keep track of the rover's total movement from its starting position.

We will define two such locally fixed frames: `odom` and `map`. We will use the `map` frame to keep track of the position estimate of the rover using all available sensors, including GPS. The GPS measurements filtered through the EKF will cause this estimate to jump around erratically, making it discontinuous. We will use the `odom` frame to keep track of the position estimate of the rover, using all sensors except for the GPS. This position estimate will be smooth and continuous, but the position error will grow unbounded over time.

The UTM (Universal Transverse Mercator) frame defines a frame equal to the axes used by the UTM zone that the rover is currently in. The origin is at the (0,0) point of the UTM zone, and the axes are oriented according to the ENU convention. See Figure 4-1 for a graphical representation of the UTM frame compared to the other frames. The figure shows the rover at time $t = 0$, right at the start of localization. Notice that the `base_link`, `odom`, and `map` frames are all aligned. The phone frame, not pictured, would have the same origin as those three, but its axes would be oriented parallel to the UTM frame's axes. As the rover moves, the `base_link` and phone frames would

Figure 4-1: [robot_localization_wiki]



move with it. The base_link axes would rotate as the rover rotates, and the phone axes would remain oriented as ENU. The odom and map frames would stay fixed at where they began.

As the rover localizes, it calculates its position with respect to the odom, map, and utm frames. Odometry data coming from the wheel encoders is reported with respect to the base_link frame, while IMU and GPS sensor data from the phone is reported w.r.t. the phone frame. For the rover to fuse this data together, it needs to transform it into the equivalent information in one of the fixed frames: odom or map.

ROS supplies convenient tools for handling these transforms. The *tf* package allows nodes to broadcast transform definitions through the ROS network. See Figure

4-2 for a map of all transforms broadcast in this system, where arrows indicate a transform converting a parent frame to a child frame.

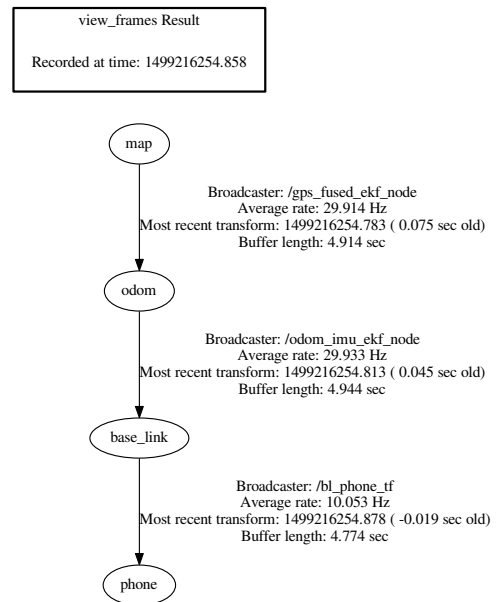
4.2 rosserial

Communication between the Arduino and laptop is handled by the ROS meta-

package rosserial. Different client packages support different client machines, such as embedded linux devices, or different microcontroller boards. These client packages create local support libraries or header files on those machines, which use a serialization protocol to send and receive ROS messages over a serial port.

On the other side of the serial connection, host packages run a bridging node which communicates with the ROS network on behalf of the client machine. Subscribed topics have their messages serialized and sent to the client machine, and outgoing messages from the client are de-serialized and published.

Figure 4-2: Transforms



4.2.1 rosserial_arduino

rosserial_arduino is one client package of rosserial, which creates an Arduino library to provide bare-bones ROS support to sketches. The sketch running on this project's Uno board uses this library to publish sensor data in ROS messages, and subscribe to motor command topics.

Every time the sketch wishes to update the laptop with its newest sensor readings, it publishes three messages. First the servo angle in degrees is published to the "/ping/angleDeg" topic, as a standard Int8 message. This message just contains a single data field: an 8-bit signed integer. Next the echo time in microseconds is published to the "/ping/timeUS" topic, as a standard UInt16 message which contains a single 16 bit data field representing an unsigned integer. Lastly the two encoder tick counts are both placed into a single custom message called EncCount, and published to the "/odom/encTicks" topic. This custom message type has two 32 bit fields, one for each encoder.

When the sketch is waiting between updates, it continually listens to the serial port for motor commands. These commands are Int8 messages on the "/cmd/left" or "/cmd/right" topics, which the sketch subscribes to. When these messages are found in the serial input buffer, a short callback function is executed, which writes the R/C pulse command to the proper motor channel.

Arduino boards use different types of memory. Flash memory is used to store compiled code, and static random access memory (SRAM) is used to store dynamic variables at runtime. The Uno has 32kB of flash memory, but only 2kB of SRAM.

The rosserial Arduino library is large, and takes up quite a lot of SRAM space. Its input and output serial buffers alone use 1024 bytes in total. This makes running out of space for local variables quite easy, which can lead to instability and crashes when running the sketch. To save space, a modified version of `rosserial_arduino` has been used, which supports storing constant strings in flash memory rather than SRAM. Since topic names and error messages use long descriptive strings, this saves several hundred kB of space in SRAM and ensures the sketch's stability.

The rosserial Arduino library abstracts away most of the serial communication protocol, but does allow the baud rate to be specified. In this use case, baud rate is equivalent to bits per second. The more bits per second sent over serial, the more frequently the microcontroller needs to sample the incoming and outgoing line. So the baud rate cannot be set arbitrarily high, as the Uno has a limited clock speed. If it is set too low, however, then the stream of sensor data being published would overwhelm the connection. Significantly less data will be streaming in than transmitted out, so the amount of outgoing data is the deciding factor. Thus to calculate an appropriate baud rate, the amount of sensor data transmitted per second must be known.

rosserial uses a serial protocol with 8 bytes of overhead for every message. Each sensor update publishes three messages: an eight-byte EncCount message, a one-byte Int8 message, and a two-byte UInt16 message. This means that each update pushes 11 bytes of data in three messages, with 24 bytes of overhead. Thus a total of 35 bytes are sent over serial.

Since the PING))) sensor requires a minimum delay of 30 ms between pings, the sketch cannot publish its sensor values at a rate higher than 33 Hz. Therefore the

sketch will not push more than:

$$33 \text{ Hz} * 35 \text{ Bytes} = 1155 \text{ Bytes per second (Bps)}$$

The Uno uses one start bit and one stop bit to surround each byte of information sent over serial. Thus it takes 10 bits to send one byte of information. Therefore the minimum baud rate required is:

$$1155 \text{ Bps} * 10 \text{ bits per byte} = 11550 \text{ bits per second}$$

We choose a standard baud rate of 28,800 to more than double that for some breathing room, and to account for the fact that the rosserial Arduino library occasionally transmits time-keeping and synchronization messages of its own.

4.2.2 rosserial_python

rosserial_python is one host package of rosserial, which acts as a bridge between the Arduino and ROS network. It runs a node on the laptop which communicates with the Arduino using the rosserial protocol. It automatically handles setup, communication with the ROS Master, and subscription and publishing on behalf of the Arduino. When launched, the serial node must be configured to use the same baud rate as the Arduino: 28,800. It must also be configured to connect to whichever serial port name the Arduino uses. For simplicity, a symbolic link was created using Ubuntu's udev rules, to ensure that the port name will always be accessible as "/dev/arduino".

4.3 differential_drive

The differential_drive package was created by Jon Stephan to create a simple interface for controlling a differential wheeled robot [**differentialDrivePackage**]. Such a robot uses a two-wheeled system where both wheels are on a common axis, but each wheel is driven independently. Turning is achieved by lowering the velocity of one wheel compared to the other.

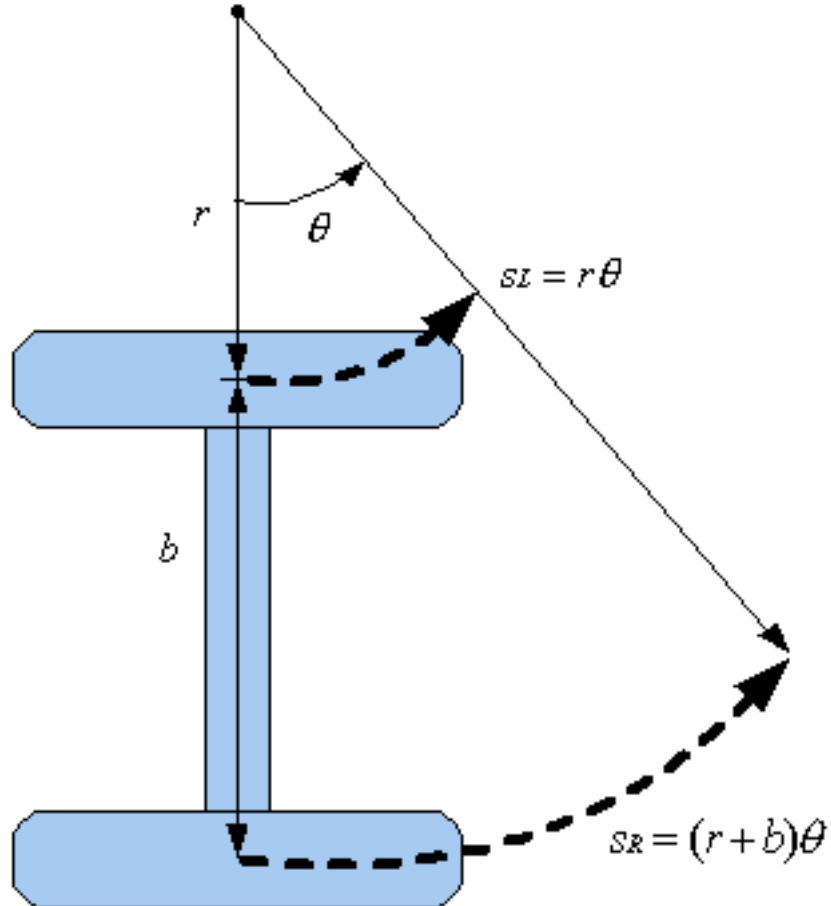
Because the rover has four wheels, turning necessarily involves slippage of one or more wheels. This is known as a skid-steering system, due to the skidding of the wheels. When wheels slip, they move without rotating. The motor encoders cannot see this movement, and so this causes error in the wheel odometry estimate. This error makes it difficult to properly localize the rover, especially with respect to the rover's heading. Despite this flaw, this package was used to model the rover as a differentially steered robot for the purposes of dead reckoning, due to the lack of ROS support for skid-steering vehicles.

4.3.1 diff_odom

Odometry messages are a type of ROS message used for navigation. They represent an estimate of the position and velocity of the rover at a certain time. The diff_odom node subscribes to encoder tick data, and uses that data to calculate and publish an Odometry message to the "odometry/wheel" topic. The Odometry messages contain estimates of the rover's position, orientation, and linear and angular velocity with a timestamp. This node is a modified version of the diff_tf node from the differen-

tial _drive package, which was changed to use the custom EncCount message type, set appropriate covariance values, and not publish an odom->base_link transform. That transform is published by the EKF node after fusing all sensor data, as will be described in section 4.5.

Figure 4-3: [differentialSteeringPaper]



To understand how the diff_odom node calculates its odometry estimate, let us take a look at the standard theory for differential wheeled robots. Figure 4-3 shows a simple two-wheeled robot making a left turn of θ radians around some point. We assume the robot is one rigid body, and that each wheel maintains a constant velocity along the turn. This assumption of zero acceleration is obviously violated in the

real world, but robots with a small mass and relatively powerful motors are able to approximate it well. [[differentialSteeringPaper](#)]

r is the turning radius for the left wheel, and $(r + b)$ is the turning radius for the right wheel, where b is the distance between wheels. Using the formula for arc length, we know the distance traveled by the right and left wheels. Define these to be s_L and s_R . Then let point M be the midpoint of the axle between both wheels. This point will travel an arc length of $(r + (b/2))\theta$. We can manipulate s_L and s_R to produce the following two equations.

$$s_M = ((r + (b/2))\theta) = \frac{(2r + b)\theta}{2} = \frac{(r + b)\theta + r\theta}{2} = \frac{(s_L + s_R)}{2} \quad (4.1)$$

$$\theta = \frac{b\theta}{b} = \frac{(b + r - r)\theta}{b} = \frac{((r + b)\theta - r\theta)}{b} = \frac{(s_R - s_L)}{b} \quad (4.2)$$

Equation 4.1 gives the distance the center of the robot travels over the turn, in terms of the distance the two wheels traveled. Dividing this distance by the elapsed time it took to make the turn, gives an estimate of the instantaneous velocity of the robot at the end of the turn. Similarly, equation 4.2 calculates the angle of the turn using the distance the two wheels traveled. Dividing θ by the elapsed time gives the angular velocity of the robot.

Both calculations make use of the distance traveled by the two wheels. The two motor encoders attached to the rover's front wheels report a known number of ticks per revolution, and the wheel circumference can be calculated from the wheel diameter. Thus the distance each wheel travels can be computed using the difference

of encoder ticks between sensor updates. The `diff_odom` node uses these distances and equations 4.1 and 4.2 to calculate the rover's angular and linear velocity. Only the angular velocity along the rover's Z axis is reported; the wheel odometry says nothing about the angular velocity along the other axes. Because a differentially steered robot can only move in the direction of its fixed wheels, the linear velocity is reported along the `base_link` X axis, which faces forward from the rover's midpoint.

The Odometry message published includes a 6×6 covariance matrix for the linear and angular velocities along all three axes. These covariances will give the EKF an idea of how much confidence to place in these velocity estimates. Since only two velocities are calculated, constant squared variances are hard-coded in for those two variables along the matrix diagonal. Every other element in the covariance matrix is set to zero. The Odometry message also includes a pose element, which is a position in the `odom` frame. However, due to the inaccuracy of the differential drive approximation made, this estimate quickly becomes rather useless. So the EKF is configured to ignore the pose from this Odometry message completely. The odometry messages are published at a rate equal to the Arduino's sensor update rate: 10 Hz. If it were published at a slower rate, then some resolution would be lost as encoder tick messages would be skipped over.

Though the number of encoder ticks per meter may be calculated from the encoders' specification and the diameter of the wheels, it is a good idea to manually calibrate the number of encoder ticks per meter, and specify this as a configurable parameter to the `diff_odom` node. This helps account for sources of error in the physical system. The ticks per meter can easily be calibrated by moving the Arduino

one meter, and comparing the starting and ending tick count.

4.3.2 twist_to_motors

Many ROS navigation packages produce Twist messages to command robotic platforms. The Twist message includes a linear and angular velocity, which the rover is expected to match, as a subfunction of some path following algorithm. The differential_drive package uses the `twist_to_motors` node to translate Twist messages into individual motor velocities for each motor channel.

Taking into account the differentially steered conditions, this node only considers the linear velocity along the rover's x axis, and the angular velocity around the rover's z-axis. Let us refer to these as x' and θ' , respectively. Let b once again be the distance between the rover's wheels. Let L' and R' be the velocity of the left and right wheels. From equation 4.1, we know that

$$x' = (L' + R')/2$$

and from equation 4.2 we know that

$$\theta' = (R' - L')/b$$

This is a system of two equations with two unknowns, L' and R' . Solving this

system gives us:

$$L' = x' - (b * \theta')/2$$

$$R' = x' + (b * \theta')/2$$

This node uses these equations to calculate the appropriate wheel velocities from the incoming Twist message, and publishes those velocities to the "lwheel_vtarget" and "rwheel_vtarget" topics.

4.3.3 pid_velocity

The pid_velocity node creates a proportional-integral-derivative (PID) controller which uses encoder feedback to translate motor velocities into actual motor R/C pulse commands. While the appropriate R/C servo command to reach a desired velocity could be estimated from the Sabertooth motor driver's datasheet, this would be the theoretical value and would not take into account real-world sources of error such as uneven terrain, high traction, wind drag, etc. Therefore a control loop which utilizes real-time feedback is preferred.

Two of these nodes are run, one for each motor channel. One node subscribes to the topic "lwheel_vtarget", and publishes commands to "/cmd/left", while the other node subscribes to "rwheel_vtarget", and publishes to "/cmd/right". The Arduino node, through its bridge, is subscribed to these two topics and handles their messages appropriately.

PID controllers work by adjusting their output according to an error term, which

is the difference between the current feedback and the desired value. In this case the error is the difference between the wheel velocity published by the diff_odom node, and the target wheel velocity. This error, the integral of all past errors, and the instantaneous derivative of the current error are all combined into a weighted sum. This sum then acts as the new output of the system.

The weights in the sum are three constant parameters: K_p , K_i , and K_d . These parameters must be manually tuned to the target system for optimal use of the controller. The tuning procedure involves zeroing out K_i and K_d , and slowly increasing K_p until oscillation is observed in the control loop. Once a limit is found, set K_p to half of it. Then tune K_i and lastly K_d , in the same fashion.

4.3.4 virtual_joystick

For testing of the rover's localization capabilities, it was necessary to manually drive it. This was accomplished using the virtual_joystick node from the differential_drive package. To use the node, one must install PySide, the python binding for the GUI framework Qt. The node brings up a simple GUI, and allows the user to drag their mouse along a two-dimensional axis. This axis represents a desired linear and angular velocity, and the node publishes a corresponding Twist message. This node will not be needed once autonomous navigation is fully functional.

4.4 Ros Sensors App

In order to access the smartphone's IMU and GPS data, an Android app was written to act as a ROS node. All sensor messages published are from the phone's frame, which is centered 2 inches to the right of the base_link frame, and always has the ENU orientation. The app makes use of phone tethering supported by the Android OS, which allows one to access the internet over a smartphone's data plan. However, this feature is used only as a convenient way for the phone and laptop to communicate locally over USB.

4.4.1 GPS

Figure 4-4:
[GPS_trilateration]



The Global Positioning System (GPS) Trilateration was developed by the U.S. Department of Defense, and has been operational since 1995. It currently involves 31 satellites orbiting the earth in such a way that four or more satellites are always visible from

most land masses. Each satellite broadcasts a signal via radio wave, which contains the exact time the signal was sent, as well as orbital information about the exact position of the satellite at that time. When a GPS receiver reads one of these signals, it looks at the current time and calculates the length of time the signal took to reach the receiver. It can then multiply this length by the speed of light to calculate the distance between the receiver and satellite. This distance can be thought

of as the radius of a sphere centered at the satellite. The receiver must be somewhere on that sphere. Because four spheres can only intersect at one point, if the receiver knows its distance from four satellites, then it can calculate the intersection point - its location with respect to the earth. This process is known as trilateration.

[GPS_trilateration]

The GPS coordinates reported by the phone node are acquired using assisted GPS (AGPS). In AGPS, cell phone towers use a phone's signal strength to help determine its position. This provides quicker and more precise location tracking. At greater cost, one could purchase GPS hardware to access gps fix messages broadcast by the coastguard for even greater precision.

The phone node publishes gps messages as they come in: roughly every five seconds. The covariance matrix is filled in along the diagonal, using the variances reported by the Android OS.

4.4.2 IMU

Inertial Measurement Units (IMUs) are small chips that measure linear and angular movement. A digital accelerometer measures linear acceleration in all three dimensions, while a digital gyroscope measures angular velocity around each axis. Lastly, a digital magnetometer measures magnetic strength along each axis. IMU chips often report their data in the NED (North-East-Down) orientation, however the Android API reports values using the ENU convention, as expected. A covariance matrix was once again filled out on only the diagonals, with squared variances hard-coded at

reasonable estimates. All of this information is encapsulated in a ROS IMU message, which is published at approximately 5 Hz.

4.5 robot_localization

This package created by Tom Moore

implements the extended Kalman Fil-

ter, which was derived in section

1.3. The filter keeps track of a

15-dimensional vector describing the

rover's state: $(x, y, z, \Phi, \theta, \Psi, x', y', z', \Phi', \theta', \Psi', x'', y'', z'')$

[[robot_localization_paper](#)]. In this state vector Φ , θ , and Ψ represent roll, pitch, and yaw respectively. These Euler angles describe rotation about the X, Y, and Z axes. See Figure 4-5 for an illustration.

This project takes advantage of the fact that the rover is a ground vehicle and makes the assumption that all terrain is perfectly flat, and that the rover is moving in a two-dimensional environment. Thus z, roll, pitch, and their derivatives in the state vector are fixed at 0. This configuration should be changed for more elaborate testing, however this assumption eliminates an entire axis of noise from GPS altitude and IMU measurements.

Table 4.1 shows which state variables each sensor affects, where a 1 indicates that the sensor gives a reading for the corresponding state variable, and a 0 indicates that it does not.

Figure 4-5: Roll, Pitch, and Yaw
[[fig_rpy](#)]

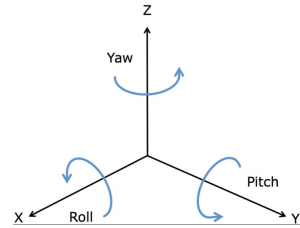


Table 4.1: Sensor Configurations [**robot_localization_paper**]

Sensor \ State Variable	x	y	z	Φ	θ	Ψ	x'	y'	z'	Φ'	θ'	Ψ'	x''	y''	z''
Sensor															
Wheel Encoders	0	0	0	0	0	0	1	0	0	0	0	1	0	0	0
IMU	0	0	0	0	0	0	0	0	0	1	1	1	1	1	0
GPS	1	1	0	0	0	0	0	0	0	0	0	0	0	0	0

The rover's system runs three nodes from this package. The first node runs an EKF which fuses wheel odometry from the diff_odom node (section 4.3.1) with IMU data from the phone node. It produces a state estimate in the odom frame.

The second node provides a helper service that transforms gps coordinates into a locally fixed frame, and vice versa. Its main use is to transform gps messages coming from the phone node into coordinates in the map frame.

The third and final node runs another EKF which fuses the odometry output from the first and second nodes together, producing a final state estimate in the map frame. This estimate is discontinuous, as the output from the second node is positional coordinates, which this node uses to instantaneously adjust the rover's x and y state variables.

Chapter 5

Field Test

In order to test the rover's ability to localize itself, a simple field test was conducted in a parking lot. Inspiration for this experiment comes from Moore and Stouch [[robot_localization_paper](#)].

5.1 Experiment Design

The rover was initially placed in a parking lot oriented westwards. It was then driven in a loop around the lot using the virtual_joystick node, described in section 4.3.4.

See Figure 5-1 for two representations of the path taken. Figure 5-1a displays the path actually traversed, while Figure 5-1b is constructed from the phone's GPS readings.

Note that despite Figure 5-1b, at no point did the rover go onto the grass. The rover was driven so that its initial and ending position and orientation were roughly equal.

Total collection time was five and a half minutes.

While the rover moved, raw sensor data streaming in from the Arduino and smart-

phone was recorded and saved into a ROS bag file. Later, the *rosbag* utility was used to repeatedly simulate the recorded sensor messages, while the EKF was run in different configurations. The rover's state was first computed from raw wheel odometry, then from wheel odometry fused with IMU data, and lastly from wheel odometry, IMU data, and GPS fixes all together. Refer to Table 4.1 for a review of which state variables each sensor affects.

5.2 Results

During each filter computation, a state estimate was produced at 30 Hz in a local frame, and that output was then transformed into the global UTM frame, where position is given as latitude and longitude. These gps coordinates were plotted using the handy GPS Visualizer tool [**gps_visualizer**] to generate the plots in Figure 5-2.

Figure 5-2a shows the estimated path when fusing only the wheel encoder odometry. The initial trajectory heading north and the subsequent turn westward is tracked reasonably well, but the second turn rotates too far and throws the rest of the estimate off.

Figure 5-2b shows the path generated when fusing wheel odometry with IMU data. In this case the shape of the path is much closer to truth, though the initial northern trajectory is under-estimated.

Lastly, Figure 5-2c shows the result of fusing both prior sensors with GPS fixes. This plot looks much like the raw gps plot in Figure 5-1b, however upon close inspection one can see jagged jumps in position. These jumps are instantaneous and actually

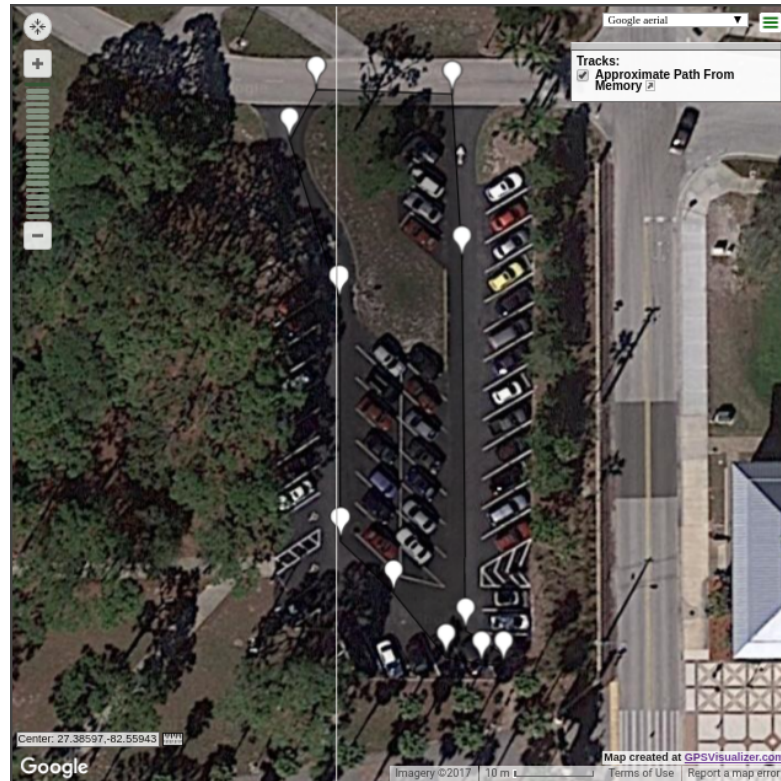
lead to a discontinuous position estimate, though the visualizing tool connects every point. They are caused by the filter instantaneously adjusting the position estimate based on incoming gps fixes. The filter gives some weight to the current estimate, so the new adjusted position lies in between the position reported by the gps fix and the current estimate. Due to the frequent gps fixes and slow velocity of the rover, the estimated path never varies too far from the raw gps path.

Table 5.1: Errors for Different Sensor Fusions [[robot_localization_paper](#)]

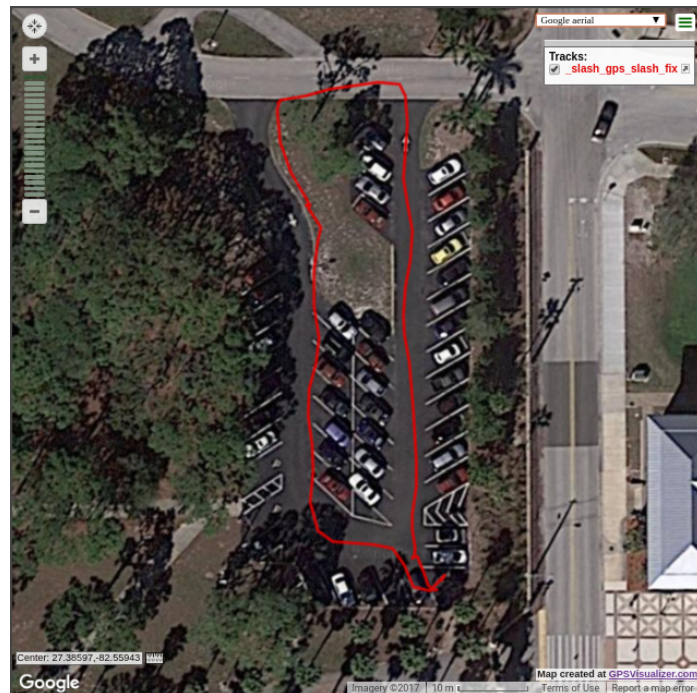
Sensors Fused	Loop Closure Error x,y (m)	Std. Dev. x,y (m)
Wheel Encoders	-88.37, -43.10	45.64, 126.36
Encoders + IMU	-12.90, -11.89	52.80, 52.02
Encoders + IMU + GPS	-0.97, -0.50	4.68, 4.56

Table 5.1 shows the position error between the rover's start and end positions for each filter configuration. Because the rover's local frame has its origin at the start point, this error is simply the last state estimate produced by the filter. The standard deviation for each dimension is also reported, giving an idea of the filter's confidence in its location. Note that the position errors are negative because the filter considers the end point to be in the -X and -Y direction of the rover's starting orientation. Recall that according to ROS convention, this translates to being behind and to the right of the starting position. This makes sense because the rover started facing west.

Figure 5-1: The rover's path.

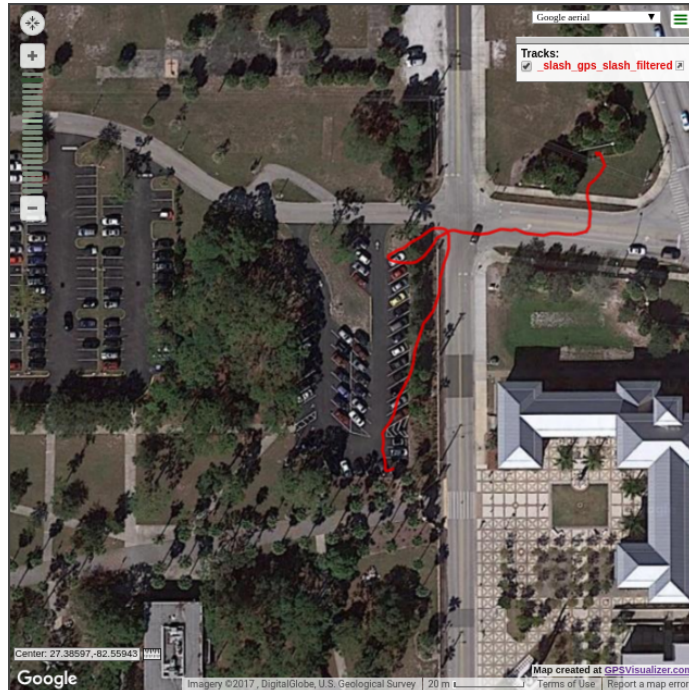


(a) Path Manually Mapped



(b) Path According to Phone's GPS

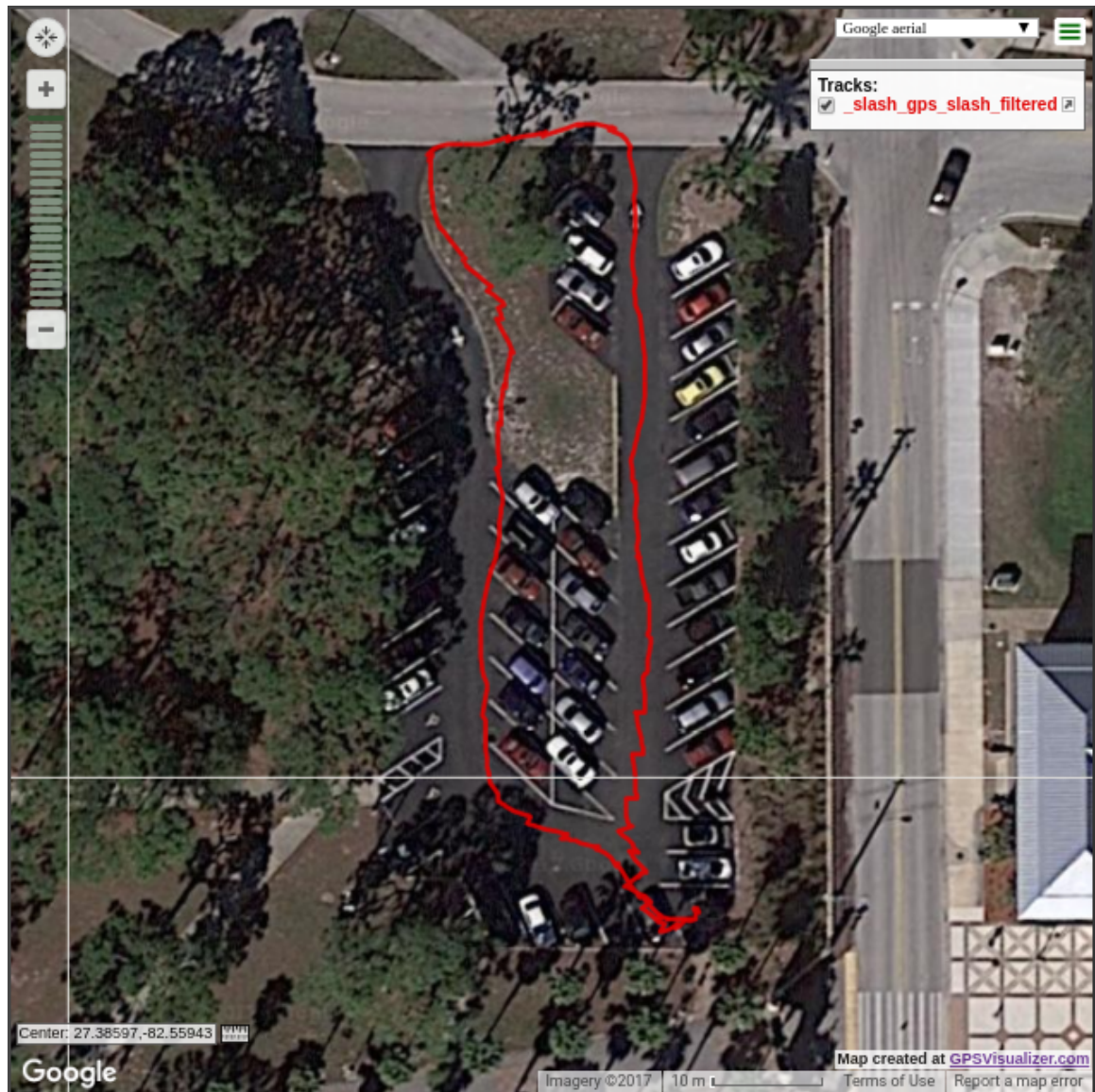
Figure 5-2: Filter Outputs For Different Sensor Fusions



(a) Raw Wheel Odometry



(b) Wheel Odometry + IMU



(c) Wheel Odometry + IMU + GPS

Conclusion

We have shown that the proposed vehicle design is capable of using wheel encoders and a smartphone to localize itself with respect to UTM coordinates.

However, this localization is less precise than it could be, due to several flaws in the rover's design. The differential drive model is a simple approximation to the skid steering rover, causing large errors in the yaw state variable to accumulate quickly in the wheel odometry. The covariance matrices for the sensors are hard-coded rather than dynamically computed, and need to at least be empirically calibrated. And the magnetometer readings are affected by the magnetic field generated by the DC motors. This effect could be alleviated by adding a second level on top of the rover, putting more distance between the smartphone and motors.

It is hoped that this project will be a jumping off point for future work. The logical next step would be to integrate the ultrasonic sensor's range and angle data into the project, as a slower approximation of LIDAR range data, which will allow the system to dynamically generate a map of the immediate area around the rover. Localization can then be performed in real-time with respect to this map.

Another possible extension would be to add video feed as a new source of sensor

data, either via the laptop's webcam or the smartphone's built-in camera. The camera would need shock absorbers, or else the video frames would wobble. Perhaps video stabilization techniques could be used to compensate for this, in which case visual odometry could prove useful. The Arduino microcontroller board chosen in this design could be replaced with a larger model, or by a Raspberry Pi, which is a system on a chip that costs - at the time of this writing - roughly \$15 more than the Arduino board, but comes with additional features such as built-in WiFi and Bluetooth for short-range communication.

On the software side, the differential_drive package should eventually be replaced by the diff_drive_controller package, which performs the same function but integrates more naturally into the ROS navigation stack. The collection of software used in this project is available online at the following url: [https://github.com/NoahRJohnson/](https://github.com/NoahRJohnson/AutoRover) AutoRover.